MaskFaceGAN: High Resolution Face Editing with Masked GAN Latent Code Optimization

Martin Pernuš, *Student Member, IEEE,* Vitomir Štruc, *Senior Member, IEEE,* and Simon Dobrišek, *Member, IEEE*

Fig. 1: This paper introduces MaskFaceGAN, a novel approach to face attribute editing capable of generating high-resolution, artefact-free and photo-realistic editing results through a carefully designed optimization procedure applied over the StyleGAN2 latent space. The presented (1024×1024) examples show editing results for four target attributes. Best viewed zoomed-in.

***Abstract*—Face editing represents a popular research topic within the computer vision and image processing communities. While significant progress has been made recently in this area, existing solutions: (i) are still largely focused on low-resolution images, (ii) often generate editing results with visual artefacts, or (iii) lack fine-grained control and alter multiple (entangled) attributes at once, when trying to generate the desired facial semantics. In this paper, we aim to address these issues though a novel attribute editing approach called MaskFaceGAN. The proposed approach is based on an optimization procedure that directly optimizes the latent code of a pre-trained (state-of-the-art) Generative Adversarial Network (i.e., StyleGAN2) with respect to several constraints that ensure: (i) preservation of relevant image content, (ii) generation of the targeted facial attributes, and (iii) spatially–selective treatment of local image areas. The constraints are enforced with the help of an (differentiable) attribute classifier and face parser that provide the necessary reference information for the optimization procedure. MaskFaceGAN is evaluated in extensive experiments on the CelebA-HQ, Helen and SiblingsDB-HQf datasets and in comparison with several state-of-the-art techniques from the literature, i.e., StarGAN, AttGAN, STGAN, and two versions of InterFaceGAN. Our experimental results show that the proposed approach is able to edit face images with respect to several facial attributes with unprecedented image quality and at high-resolutions (1024×1024), while exhibiting considerably less problems with attribute entanglement than competing solutions. The source code is made freely available from: https://github.com/MartinPernus/MaskFaceGAN.**

***Index Terms*—facial attribute editing, generative adversarial network, GAN inversion, latent code optimization.**

I. Introduction

FACE ATTRIBUTE EDITING refers to the task of manipulating facial images towards some predefined appearance. Techniques capable of automatically edit facial attributes (e.g., hair color, makeup, shape of facial components, age, identity) have important real-world applications not only in the entertainment, arts, the beauty and fashion industries, but also in problem domains related to visual privacy or security [1], [2], [3], [4]. As result, considerable research effort has been directed towards face editing techniques over the years and resulted in powerful techniques capable of generating convincing photo-realistic editing results [5], [6], [7], [8], [9].

Recent progress in face attribute editing has been largely driven by advances in convolutional neural networks (CNNs) and adversarial training objectives utilized in Generative Adversarial Network (GAN) models [10]. Existing solutions can broadly be categorized into two main groups. The *first* includes techniques that pose attribute editing as an *image-to-image* translation task and utilize dedicated learning objective to generate the desired target semantics [11], [12], [5], [7], [8]. Such techniques typically rely on some sort of encoder-decoder architecture and are, therefore, computationally efficient, but primarily designed for low-resolution editing (e.g., 128×128 or 256×256). Moreover, due to the nature of the learning objective used, they often induce visual artefacts in the edited images. The *second* (more recent) group of techniques is based the concept of *GAN inversion* [13] and exploits the generative capabilities of pre-trained GAN models [14], [15], [16]. With this approach a target image is first converted (embedded) into a latent code and then edited through manipulations (optimization) in the latent space. The main advantage of these techniques is the high-resolution and impressive image quality of the editing results. However, because the latent code is a global image representation with entangled attribute information, it is challenging to manipulate individual facial attributes without affecting others.

In this paper we propose a novel GAN-inversion based approach to facial attribute editing, called MaskFaceGAN, that is capable of generating high-resolution visually convincing

editing results (illustrated in Fig. 1), and does not suffer from the entanglement problems discussed above. At the core of the approach is a carefully designed optimization procedure operating directly over the latent space of the recent StyleGAN2 model [17]. The procedure aims to determine a latent code that encodes the desired target semantics (i.e., presence/absence of a target attribute and original facial appearance) by considering multiple groups of optimization constraints during the process of GAN inversion. The *first* group is enforced through a facial attribute classifier and ensures that the edited image contains the correct attribute information. The *second* group of constraints is imposed through a face parser that defines image regions that belong to different facial components. Information on these components is then used as the basis for spatial constraints that encourage the optimization procedure to either preserve or alter image regions corresponding to specific facial regions. We evaluate MaskFaceGAN on three high-resolution face datasets and in comparison to several state-of-the-art editing techniques from the literature. The results of rigorous (qualitative and quantitative) experiments show that the proposed approach generates highly competitive editing results in comparison to the state-of-the-art, while exhibiting some uniquq characteristics not available with previous methods in this area.

All in all, we make the following contributions in this paper:

- We present MaskFaceGAN, a novel approach to face image editing, capable of generating state-of-the-art, visually convincing, artefact-free, photo-realistic editing results at high resolutions, i.e., 1024×1024 pixels.
- We propose an efficient optimization procedure for estimating latent codes of GAN models encoding selected target semantics. The procedure enforces various optimization constraints through the use of differentiable models applied over the edited images.
- We show how MaskFaceGAN can be used for attribute-intensity control, multi-attribute editing and component size manipulation while requiring only binary attribute labels for optimization.
- Through rigorous comparative evaluations with the state-of-the-art, we demonstrate that spatially constrained image editing contributes to considerable mitigating entanglement problems when compared to competing models.

II. Related work

In this section we present prior work closely related to our paper. We discuss Generative Adversarial Networks (GANs), research on pre–trained GANs and face editing techniques.

A. Generative Adversarial Networks

Generative Adversarial Networks (GANs) are among the most popular generative models in the field of image processing and computer vision [10]. Existing GANs can be broadly split into two categories: (i) unconditional and (ii) conditional models. Unconditional GANs refer to models that rely on random noise only to generate image data, no additional signal is used to steer the generation process. Conditional GANs, on the other hand, exploit an additional input to control the semantic content of the generated images and typically utilize random noise to ensure diversity. Different forms of the conditional signals have been used successfully in the literature, including class labels [18], [19], graph representations, [20], [21], layouts of image objects [22] or text descriptions [23], [24], [25] among others.

The progress in GAN-based image generation has largely been driven by advances in model design and training. DCGAN [26], for example, proposed a convolutional GAN architecture and defined several useful design principles, such as the use of batch normalization in all model layers and specific activation functions for the generator and the discriminator of the model. Karras et al.[27] introduced a progressive learning strategy for GAN models that adds higher resolution layers to the model once the lower resolution layers converge. The authors showed that using such a strategy results in GAN models capable of generating convincing megapixel-sized images. The progressively learned model was further improved with the introduction of StyleGAN [28], where the model architecture was inspired by the style–transfer literature. Different from traditional Gaussian-shaped latent spaces, StyleGAN proposed the use of a non-linear mapping from the Gaussian latent space to an intermediate latent space that is then fed to convolutional layers via an adaptive instance normalization operation. The intermediate latent space demonstrated better interpolation and disentanglement properties. Additionally, the model also introduced noise inputs as a means to generate stochastic details in the images. The next iteration of the model, called StyleGAN2 [17], modified the adaptive instance normalization operation to remove circular artefacts in the generated images, achieving state of the art results on unconditional image generation. Considerable progress has also been made with the strategies utilized for learning GAN models, where different losses and regularizations were proposed to improve the generation quality [29], [30], [31], [32], [33]. Additional information on GANs can be found in one of the existing surveys on this topic [34], [35].

B. Studies on Pre-trained GANs

Training of GAN models can be highly resource intensive. For example, the computational effort required for developing and training the recent StyleGAN2 model is estimated to be around 51 Volta GPU years [17]. This effort has motivated research into the capabilities of pre–trained GANs and resulted in powerful techniques that exploit existing models for various generative image processing tasks. Bau et al. [36], for example, analyzed a pre–trained GAN to achieve localized deletion and insertion of objects. Jahanian et al. [37] investigated linear and non-linear walks in the GAN latent space that achieved basic image manipulations, such as changes in brightness or in the zoom factor. Goetschalckx et al. [38] navigated the latent code manifold to improve the image's memorability. Yang et al. [39] analyzed the relationship between image semantics and layer activations and based on the findings were able to edit various image attributes, such as layout, scene attributes and the employed color scheme.

Similar to the research discussed above, we also exploit a pre-trained GAN model to edit facial images. Different from

existing work, the GAN model used in our framework serves only as a proxy for the editing procedure that synthesizes semantically meaningful facial regions in spatially local image areas. As result of this process, our approach inherits the characteristics of the adopted GAN model and is able to generate convincing artifact–free facial images at high-resolutions.

C. Face Editing

Numerous approaches for face editing and manipulation have been presented in the literature [1], [2], [40], [41]. The work in [42], [6], for example, explored the use of user-supplied sketches to drive the editing procedure. The authors of [11], [12] learned disentangled latent representations with respect to image formation with the goal of steering the image generation process. Lee et al. [43] proposed MaskGAN model, a conditional GAN architecture, capable of modifying specific facial components and demonstrated the benefit of using spatially local facial editing.

Particularly convincing editing results have been achieved with encoder-decoder models. Choi et al. [5], for instance, introduced StarGAN , a multi-domain image-to-image encoder-decoder network with cycle consistency [44], capable of manipulating the appearance of several face attributes. He et al. [7] proposed AttGAN, a notable encoder-decoder model that relies on a reconstruction constraint instead of cycle consistency. Liu et al. [8] improved on AttGAN with their STGAN design by modifying the input signal and improving the encoder-decoder architecture with selective transfer units. Encoder-decoder models methods typically succeed in generating visually convincing editing results, but are less suitable for editing high-resolution images, where visual artefacts are often observed.

More recent work in this area, approaches the problem of face editing with the use of pre-trained GANs. Abdal et al. [15] showed that it is possible to embed a large variety of images in the extended latent space of StyleGAN and to perform various forms of image manipulation in the latent space, including face morphing, style transfer and expression transfer. In their follow up work [16], the authors improved the embedding algorithm by optimizing the StyleGAN noise component, and demonstrated additional capabilities, such as local editing using scribbles or face inpainting. A convincing editing approach, called InterFaceGAN, was described by Shen et al. in [9], [14]. To edit an image, InterFaceGAN moves the corresponding latent code along a linear subspace. The direction of the displacement is determined through a support vector machine, trained on the StyleGAN latent space given labels of predefined facial attributes. While the presented approaches led to state-of-the-art editing results, they are based on linear operations applied over latent space representations and, therefore, often suffer from entanglement issues where changing one attribute also results in changes in other (entangled) visual attributes.

With MaskFaceGAN we improve on previous methods by directly optimizing the latent code associated with an input image through multiple optimization objectives that not only control the manipulated semantic content but also the spatial area in which the editing occurs. This optimization procedure results in complex (non-linear) changes in the latent code of the input image and leads to editing results with significantly less entanglement problems than competing solutions, as we demonstrate in the experimental section.

III. Methodology

In this section we now present the proposed MaskFaceGAN face editing approach. We start the section with a description of the theoretical background of editing techniques based on latent code optimization and then proceed with an in–depth discussion of MaskFaceGAN.

A. Background and Problem Formulation

Face attribute editing represents a challenging computer vision task, where the goal is to edit (in a photo–realistic manner) a given input image $I \in \mathbb{R}^{3\times m\times n}$ in accordance with some target semantics a, i.e.,

$$\psi_a : I \mapsto I' \in \mathbb{R}^{3\times m\times n}, \tag{1}$$

where I' represents the edited image and the semantics are usually defined by predefined facial attributes (e.g., "Blond hair", "Big nose", etc.). As discussed in the previous section, existing editing techniques implement the mapping ψ_a through various CNN models and more recently also through so–called GAN inversion techniques [14]. With these techniques the input image I is first embedded in the latent space of the given GAN model G, resulting in a latent representation (or latent code) w. Next, the latent code is modified in accordance with a target objective determined by a, i.e., $\psi_a : w \mapsto w^*$, and finally, the the edited image I' is generated by evaluating w^* through G, that is, $I' = G(w^*)$.

MaskFaceGAN, presented in the following sections, follows this general GAN inversion framework, but different from competing solutions: (i) does not require to embed the image first, but edits the image according to target semantics in the GAN inversion optimization procedure itself, (ii) proposes a novel method for adding semantic and spatial constraints during the GAN inversion method, (iii) allows advanced editing techniques, such as simultaneously controlling the semantics intensity while changing the target face region.

B. Overview of MaskFaceGAN

A high–level overview of MaskFaceGAN attribute is presented in Fig. 2. At the heart of the proposed editing procedure is a latent–code optimization procedure that differently from existing solutions does not embed the whole image I into the GAN latent space, but only focuses on a local face region associated with the targeted semantics. Several constraints are imposed on the latent code during optimization, including: (i) an *appearance–preservation constraint* that ensures that the edited image I' is as close to the original I in image areas that should not be altered by MaskFaceGAN, (ii) a *semantic constraint* that ensures meaningful target semantics within local image areas, and (iii) a *shape constraint* that determines the image regions to be manipulated by the editing procedure.

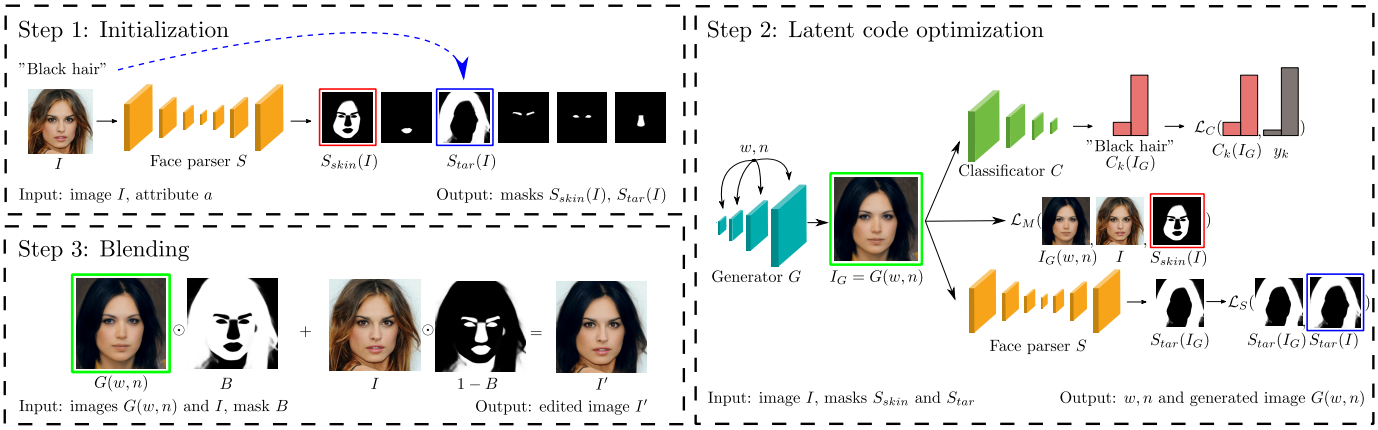

Fig. 2: Overview of the proposed MaskFaceGAN face editing approach – illustrated with the "Black hair" target attribute. To initialize the procedure, MaskFaceGAN uses a face parser to define masks that correspond to image regions that should be preserved (S_{skin}) and regions that can be altered (S_{tar}). Next, latent code optimization is performed in accordance with appearance–preservation, semantic and spatial constraints to generate an intermediate image I_G with the targeted characteristics. Finally, blending is used to combine the generated intermediate image I_G with the original one I to produce the final editing result of MaskFaceGAN I'. The image is best viewed electronically and in color.

The outlined optimization procedure is used within a three–step procedure, when editing images with MaskFaceGAN, i.e.:

- **Step 1: Initialization.** Given an input image I and a binary (target) attribute label a, MaskFaceGAN uses a face parser S in the first step to identify facial regions S_{skin} that should be preserved during editing and predict image areas S_{tar} to be edited given a. See Fig. 2 for an example using the target attribute "Black hair".
- **Step 2: Latent–code optimization.** The (main) second step of MaskFaceGAN involves the optimization of the GAN latent code. This step aims to determine a latent representation corresponding to an image I_G with the targeted semantics in image regions defined by S_{tar} and preserved appearance in S_{skin}. The semantics are enforced through an attribute classifier C and the spatial constraints through a face parser S. A loss is defined over these models and backpropagated to the latent space to facilitate the optimization.
- **Step 3: Blending.** Finally, a blending step is utilized to combine the image generated from the optimized latent code I_G (with locally manipulated target semantics) with the original image I. This step adds the background and other facial components that were not considered during optimization to the final editing result I'.

As we show in the experimental section, the illustrated editing procedure is able of generating high–resolution photo–realistic image manipulations with unique characteristics when compared to competing techniques from the literature.

C. Models

MaskFaceGAN relies on three distinct components, a GAN–based generator (G) capable of producing high–resolution facial images, an attribute classifier (C) utilized for enforcing the targeted semantics, and a face parser (S) used for imposing spatial constraints.

- **The Generator** (G) is based on StyleGAN2 [17], a (recent) state of the art GAN model specialized for generating photo–realistic facial images. Following established methodology [15], [16] the extended latent space[1] $\mathcal{W}^+$ of StlyeGAN2 is used for encoding image semantics. As a result, an image is represented through a concatenation of $n_c = 18$ different 512-dimensional latent vectors w_i, one for each layer of the model, i.e., $w = \{w_i\}_{i=1}^{n_c}$. To ensure photo-realism StyleGAN2 additionally uses $N = 17$ stohastic (i.e., Gaussian noise) channels $n = \{n_i\}_{i=1}^{N}$ of different spatial resolutions (ranging from 4×4 to 1024×1024) that encode high-frequency image details. The model, hence, generates output images I_G based on the following mapping: $I_G = G(w, n)$.
- **The Attribute Classifier** (C) is designed around the multi–task tree neural network from [45]. The classifier consists of several shared layers and K classification heads (branches), one for each of the K attributes supported (for editing) by MaskFaceGAN. Given an image I_G, each classification head C_a predicts the probability of a facial attribute being present in I_G, i.e., $c_k = C_k(I')$ for the k-th attribute.
- **The Face Parser** (S) is built around DeepLabV3 [46] and provides pixel-level probability predictions for various face components. Formally, the model implements a mapping from an image I to a tensor of probabilities along the channel dimension, i.e.: $S : \mathbb{R}^{3 \times n \times m} \rightarrow [0, 1]^{L \times n \times m}$, where L is the number of parsed categories (face components). For MaskFaceGAN, two principal channels are used. The first one is the skin region, $S_{skin} \in [0, 1]^{n \times m}$, which facilitates preservation of facial characteristics unrelated to the change in the targeted semantics. The second one is determined (dynamically) based on the

[1]The extended latent space $\mathcal{W}^+$ allows for the embedding of arbitrary facial images in StyleGAN2 and represents an extension of the model's original latent space to all layers of the model.

TABLE I: Attributes supported for editing by MaskFaceGAN and corresponding facial areas manipulated by the proposed approach to enforce desired semantics.

Face attribute	Face region
Blond, Brown, Black, Grey, Straight, and Wavy hair	Hair
Wearing lipstick, Smiling, Mouth slightly open	Lower and Upper lip, Mouth
Bushy eyebrows, Arched eyebrows	Left and Right eyebrow
Pointy nose, Big nose	Nose
Narrow eyes	Left eye, Right eye

targeted facial attribute, $S_{tar}(I) \in [0,1]^{n \times m}$.

D. Supported Attributes and Local Embedding

MaskFaceGAN is designed around the assumption that changes in certain attributes are reflected only through changes in spatially local facial regions. As we demonstrate in the experimental section, this assumption is not only reasonable, but also helps to mitigate issues related to attribute entanglement often observed with competing techniques.

Based on the attribute annotations and face components available with popular face datasets, such as CelebA [47] and CelebAMask-HQ [43], we identify 14 facial attributes that can be associated with specific facial regions, as summarized in Table I. MaskFaceGAN, hence, supports editing of 14 different attributes, comparable (in terms of numbers) to competing approaches from the literature, e.g., [7], [8]. Additionally, the local nature of the editing procedure, allows MaskFaceGAN to embed only specific image regions into the StyleGAN latent space (similarly to [16]) and enforce targeted semantics only within local spatial areas. For example, we only embed the nose region when targeting the 'Pointy nose' attribute and optimize the latent code with the goal of ensuring the desired semantics exclusively within the nose area – irrespective of the visual changes to other facial parts[2]. This is achieved to through a series of carefully designed optimization objectives presented in the next section.

E. Latent Code Optimization

The key step with the MaskFaceGAN face editing approach is the optimization of the latent code w, which is performed based on multiple optimization objectives, as detailed below.

Appearance Preservation. The goal of facial attribute editing is to alter specific (targeted) image semantics, while preserving all (or most) other visual characteristics of the input images. To ensure that image regions not associated with the targeted attributes are preserved as much as possible, a (local) appearance–preservation objective is used by MaskFaceGAN. The objective is defined as a masked mean squared error, i.e.:

$$\mathcal{L}_M = ||S_{skin}(I) \odot (I_G - I)||_2^2, \tag{2}$$

where $S_{skin}(I)$ is a probabilistic mask produced by the face parser S, $\odot$ is the Hadamard product, and $I_G = G(w, n)$. $\mathcal{L}_M$ encourages the generated image I_G and the input image I to be as similar within the image area defined by S_{skin}.

Semantic Content. The optimization objective in Eq. (2) forces certain image regions in I_G to be preserved with respect I, while the rest is allowed to change. MaskFaceGAN, thus, synthesizes the remaining image pixels in accordance with the targeted semantics by considering a semantic–content objective during optimization. The objective ensures that the latent code w produces an image I_G with the desired facial attributes and is defined as the average Kullback–Leibler (KL) divergence D_{KL} between the smoothed ground truth probability distribution and classifier predictions for the targeted attribute(s) [48], i.e.:

$$\mathcal{L}_C = \frac{1}{K} \sum_{k=1}^{K} D_{KL}(C_k(I_G), y_k). \tag{3}$$

where K denotes the number of the targeted facial attributes, C_k stands for the attribute classifier prediction corresponding to the k-th attribute and $y_k \in \{\epsilon, 1-\epsilon\}$ is a smoothed ground truth value that denotes the absence or the presence of the desired attribute, respectively. The value of ϵ can be used to set the intensity of the desired attribute, e.g. the intensity of lipstick presence when editing "Wearing lipstick".

Target Region Shape. Because image content with the targeted semantics is first synthesized by MaskFaceGAN and later blended with the original image, it is critical that the shape of the targeted facial regions is preserved. To this end, the proposed approach constrains the shape of the targeted region with the help of the face parser S using the following optimization objective:

$$\mathcal{L}_S = ||S_{tar}(I) - S_{tar}(I_G)||_2^2, \tag{4}$$

where S_{tar} is again a probabilistic mask of the spatial region associated with the targeted attribute – see Table I.

Constraining the shape of the manipulated face components was found to be especially important for hair editing. If the synthesized hair in I_G does not cover at least the original hair region in I, the blending steps generates visible artefacts that affect the perceived quality of the edited images.

Component Size. While the main goal of MaskFaceGAN is to produce convincing manipulations of existing image content, additional components can be incorporated into the framework to enable further editing capabilities. Specifically, MaskFaceGAN can manipulate the size of the target facial region by considering an additional objective during the latent code optimization procedure. To this end, we first define the portion of the image $s_{tar} \in [0,1]$ covered by a given target component as:

$$s_{tar}(I) = \frac{\sum_{x,y} S_{tar}(I)}{|S_{tar}(I)|}, \tag{5}$$

where the operator $|S_{tar}(I)|$ denotes the number of pixels in S_{tar}. To be able to scale the size of the targeted facial region we introduce a scaling factor α and integrate it into an objective that considers the component size when optimizing for the latent code w. The objective is defined as the KL

[2]The modified visual information in other parts is corrected for through the blending procedure used by MaskFaceGAN.

divergence between the initial component portion $s_{tar}(I)$ and the desired portion $s_{tar}(I_G)$ in the generated image I_G, i.e.:

$$\mathcal{L}_P = D_{KL}\left(s_{tar}(I_G), \alpha s_{tar}(I)\right). \quad (6)$$

We note that this term is optional and can be excluded from the optimization procedure by setting the corresponding weighting factor to 0 - see final objective in Eq. (9) for details.

Flexible spatial constraints The appearance–preservation and target–shape optimization objectives, as defined in Eqs. (2) and (4), impose significant constraints on the spatial regions associated with the targeted facial attributes. The appearance–preservation objective does not allow to grow relevant facial components if they overlap with the skin region. Similarly, the target–shape objective forces the edited image to have exactly the same target component shape, which in some cases might not be desired. For example, when editing hair color, the target shape needs to be preserved, but when editing the hair shape (e.g., "Straight hair" or "Wavy hair") modifications of the target image region must be allowed.

To deal with such issues, we relay the strict optimization objectives from Eqs. (2) and (4) and incorporate mechanisms into MaskFaceGAN that allow for flexible spatial constraints. Specifically, in each iteration of the optimization procedure, we first compute the target region on the generated image $S_{tar}(I_G)$. Next, we subtract this region from $S_{skin}(I)$ for the appearance–preservation objective so we preserve less pixels. For the target–shape objective, the region is added to the target region of the original image $S_{tar}(I')$ to allow region growth. Here, we also require that the combined region covers at least the original component shape to avoid visual artifacts. The final (relaxed) appearance–preservation $\mathcal{L}_M$ and target–shape $\mathcal{L}_S$ optimization objectives used by MaskFaceGAN are hence defined as:

$$\mathcal{L}_M = ||\min((S_{skin}(I) - S_{tar}(I_G), 0) \odot (I_G - I)||_2^2, \quad (7)$$

and

$$\mathcal{L}_S = ||\max(S_{tar}(I) + S_{tar}(I_G), 1) - S_{tar}(I_G)||_2^2, \quad (8)$$

where $\min$ and $\max$ denote pixel–wise minimum and maximum operations. The impact of these constraints on the appearance of a few sample images is shown in Fig. 3.

Final Objective. The overall optimization objective $\mathcal{L}_w$ of MaskFaceGAN is defined as a linear combination of the objectives described above, i.e.:

$$\mathcal{L}_w = \lambda_M \mathcal{L}_M + \lambda_C \mathcal{L}_C + \lambda_S \mathcal{L}_S + \lambda_P \mathcal{L}_P, \quad (9)$$

where λ_M, λ_C, λ_S and λ_P are weighting factors the control the contribution of the individual objectives.

Minimizing $\mathcal{L}_{fin}$ leads to an optimized latent code w with respect to the targeted semantics a that can be used to generate a synthetic attribute edited image I_G.

F. Noise Component Optimization

While the semantic content of the edited images is controlled by the latent code w, the high-frequency facial details that ensure photo realism are defined by the noise components n. After the latent code w is optimized, w is frozen and

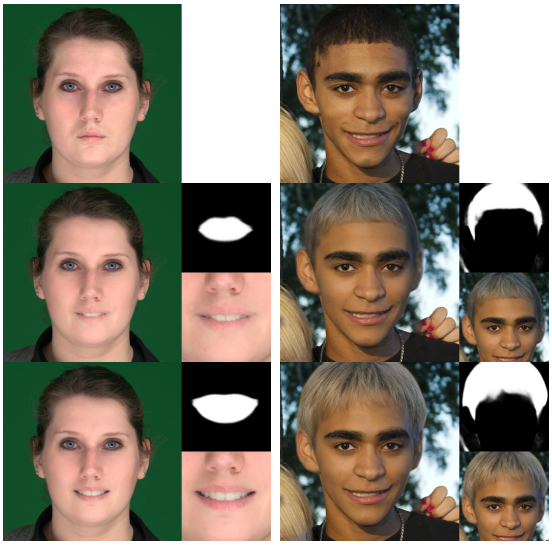

Smiling Straight hair

Fig. 3: Impact of flexible spatial constraints on the visual appearance of two sample images with two targeted attributes. The first row shows the original images, the middle row shows the editing results and the target region $S_{tar}(I)$ without flexible spatial constraints, and the final row shows the results with flexible constraints. Note how better semantics can be captured for the both the "Smiling" as well as the "Straight hair" target attributes by relaxing the spatial constraints.

MaskFaceGAN proceeds to optimize n, similarly to [16]. Two key issues are considered during optimization, i.e.:

- *Adversarial solutions:* Due to the high-dimensionality of n, a naive optimization procedure based on Eq. (10) can quickly lead editing results akin to adversarial examples, i.e., generated images that satisfy all constraints but do not exhibit the desired semantics. To avoid such settings the objectives related to semantics and target–region shape are not considered when optimizing for n.
- *Overfitting:* The optimization procedure can lead to a solution that perfectly reproduces all stochastic details of the original face (e.g., freckles, wrinkles) except for facial areas altered by the editing procedure. This mismatch between preserved and altered image regions results in unnatural appearances and a "copy-paste" look. To avoid such overfitting and ensure a reasonable amount of details in both the preserved and the generated image regions, MaskFaceGAN uses a noise regularization term similarly to [17].

Based on the above considerations, MaskFaceGAN's noise-related optimization objective takes the following form:

$$\mathcal{L}_n = \lambda_M \mathcal{L}_M + \lambda_R \sum_{i,j} L_{i,j}, \quad (10)$$

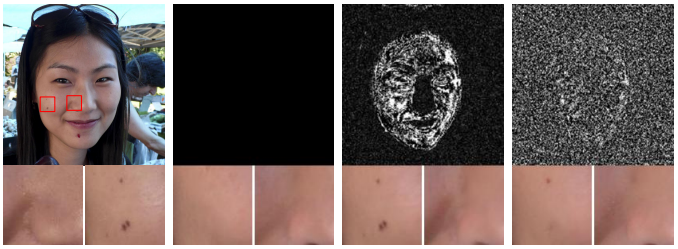

Original $n = 0$ $\lambda_R = 0$ $\lambda_R \neq 0$

Fig. 4: Embedding quality with respect to different noise optimization settings when editing an attribute associated with the nose region. The first column shows the original image and a closeup of two face regions. The second columns shows that without noise optimization high-frequency details are not embedded but smooth transitions are generated between the skin are and the nose regions. Optimizing for the noise directly perfectly embeds fine skin details, but does not produce smooth transition as seen in the third columns, while the regularization optimization generates a reasonable trade–off between details and transitions as seen in the last column.

where λ_M and λ_R are again weighting factors and the noise regularization term $L_{i,j}$ is defined as:

$$L_{i,j} = \left(\frac{1}{|n_{i,j}|} \sum_{x,y} n_{i,j}(x,y) \cdot n_{i,j}(x-1,y) \right)^2 + \left(\frac{1}{|n_{i,j}|} \sum_{x,y} n_{i,j}(x,y) \cdot n_{i,j}(x,y-1) \right)^2 . \quad (11)$$

The goal of this regularization term is to ensure that the noise components follows a normal Gaussian probability distribution by preserving the mean and standard deviations of neighbouring values. At every step of the optimization, each noise component larger than 8×8 is downsampled in a pyramid-like fashion to a resolution of 8×8 by averaging 2×2 neighbouring values. In the above equation, $n_{i,j}$, thus, denotes the i-th noise component at the original resolution ($j = 0$) or a given level of the downsampling pyramid ($j > 0$). The number of elements of $n_{i,j}$ is denoted as $|n_{i,j}|$ and the corresponding regularization term as $L_{i,j}$. The impact of the noise regularization term is illustrated in Fig. 4.

G. Blending

In the final step, MaskFaceGAN blends the image generated based on the optimized latent code w and noise components n, $I_G = G(w, n)$, with image regions in the input image I that were not consdiered during the optimization procedure. These regions corresponds to the background and non-edited facial components. To facilitate this step, a blending mask is computed as $B = S_{skin}(I) + S_{tar}(I_G)$, where the target component is predicted on the generated image to account for potential component size changes. The final image I' is then generated as

$$I' = B \odot I_G + (1 - B) \odot I. \quad (12)$$

The blending step is visualized in the bottom left of Fig. 2.

IV. Experimental Setup

In this section we present the experimental setup used for the the evaluation of the proposed MaskFaceGAN face editing approach. Specifically, the section elaborates on the datasets selected, implementation details and competing methods included in the comparative evaluations.

A. Datasets and Experimental Splits

Five datasets with high–quality (high–resolution) images are used for training and testing of MaskFaceGAN, i.e., Flickr–Faces–HQ (FFHQ) [17], CelebA [47], CelebA–HQ [43], Helen [49] and SiblingsDB–HQf [50]. The datasets are selected for the experimental evaluation based on different characteristics, such as dataset size, image resolution, image quality, and available annotations. A brief summary of the datasets and experimental splits used is given below:

- **Flickr–Faces–HQ (FFHQ)** [17] contains $70,000$ high quality face images at a resolution of 1024×1024 pixels. The images were crawled from Flickr and contain considerable variation in terms of age, ethnicity and image background. FFHQ is used to the train the generator model (G) of MaskFaceGAN.
- **CelebA** [47] is a large–scale face image dataset, consisting of more than $200,000$ celebrity images. Each image is annotated with identity information, 40 binary attributes and 5 landmark locations. CelebA is used to train the attribute classifier (C) of MaskFaceGAN in accordance with the official training and validation splits [47].
- **CelebA–HQ** [27] is a recent dataset, derived from CelebA. It consists of $30,000$ aligned, quality–improved images processed by JPEG artefact removal and super–resolution. For the experiments, the CelebAMask–HQ[3] version from [43] is utilized, which comes with pixel–level annotations of semantic face classes. CelebA–HQ is used to train the face parser (S) and to evaluate the performance of MaskFaceGAN. Training and validation sets are defined by mapping the predefined experimental splits of CelebA to CelebA–HQ images. For the quantitative evaluations (i.e., the user study), a disjoint set of 100 images is selected based on perceived face quality and data diversity.
- **Helen** [49] consists of 2330 high–quality face images annotated with facial landmark locations. In comparison to CelebA–HQ, there are considerably larger variations in age, race and lightning conditions present in this dataset, posing a greater challenge to face editing technology. 118 test images are selected for the quantiative evaluations of MaskFaceGAN based on similar criteria as discussed above for CelebA–HQ. The selected test images are manually annotated with binary attributes.
- **SiblingsDB–HQf** [50] contains frontal, expressionless images of 184 subjects – 92 sibling pairs with a resolution of 4256×2832. Images in this dataset were shot by a professional photographer in front of a uniform background and under controlled lightning. We process the

[3]We use the *CelebA–HQ* to refer to this dataset in the remainder of the paper for brevity.

TABLE II: High–level summary of the dataset and experimental setup used for training and evaluation of MaskFaceGAN. Note that datasets with different characteristics and diverse face images were selected for the experiments to demonstrate the merits of the proposed approach. The number of test images reported was used for the quantitative evaluations, e.g., the user study. The symbol "n/a" stands for *not applicable*.

Dataset	Image Resolution	Purpose	#Training Images†	#Test Images	Variability Sources
FFHQ [17]	1024×1024	Training of G	$70,000$	n/a	Age, ethnicity, background
CelebA [47]	178×218	Training of C	$182,636$	n/a	Age, ethnicity, background,accessories
CelebA–HQ [43]	1024×1024	Training of S, testing	$24,183$	100	Age, ethnicity, background, accessories
Helen [49]	> 500 in width	Testing	n/a	118	Age, ethnicity, background clutter
SiblingsDB–HQf [50]	4256×2832	Testing	n/a	163	Age, gender

† The number of training images reported includes both training and validation data.

images with the CelebA–HQ pipeline using cropping and alignment [27], then manually annotate them with binary attributes.

MaskFaceGAN is applied for attribute editing at a resolution of 1024×1024 pixels with all experimental datasets. The facial images, are, therefore, rescaled where necessary before applying the proposed MaskFaceGAN face editing approach. A high–level summary of the datasets and experimental splits is presented in Table II. Note that the reported number of test image corresponds to the amount of face imagery utilized for quantitative performance comparisons.

B. Implementation details

MaskFaceGAN is implemented using several state–of–the–art (SOTA) baseline components, i.e.:

- **The Generator** (G) of MaskFaceGAN is implemented using the powerful StyleGAN2 model [17]. To foster reproducibility, we use the official version of StyleGAN2[4] trained on images from the FFHQ dataset.
- **The Attribute Classifier** (C) is designed around the multi–task tree neural network model from [45]. The classifier is trained on CelebA [47] for 16 epochs with weighted binary cross entropy to account for the class imbalance in the training data. The learning rate is initially set to 0.05 and decayed to 0.005 on the $40,000$–th training step. The model is optimized with the Nesterov momentum algorithm [51] using a batch size of 32. To avoid over–fitting, the training data is augmented with random horizontal flipping and affine transformations.
- **The Face Parser** (S) is based on DeepLabV3 [46] and trained on the CelebA–HQ dataset to generate segmentation masks of the following seven classes: "mouth", "eyebrows", "eyes", "earrings", "hair", "noise" and "skin". Weighted cross entropy is again used as the learning objective. The model is learned using the Adam optimizer [52] with a fixed learning rate of $3 \cdot 10^{-4}$ and a batch size of 24. Learning is done for 5 epochs. We perform data augmentation with random horizontal flipping and affine transformations.

The latent code w optimization procedure is conducted in several stages. First, w is initialized with the mean latent code $\bar{w}$, computed based on $50,000$ sampled codes $w \in \mathcal{W}^+$. Next, w is optimized with respect to Eq. (2), so it approximately corresponds to the target face. This initial optimization stage was found to be important for the visual quality of the edited images. Finally, the remaining loss terms are added to enforce attribute and spatial constraints. Similarly to [16], the noise component n is set to zero and kept constant during the optimization of w. Once w converges, it is frozen and the noise component n is optimized independently of w.

To identify parameter values that yield visually pleasing editing results hyper–parameter optimization is used with MaskFaceGAN, resulting in weighting factors of $\lambda_M = 2, \lambda_C = 0.005, \lambda_S = 0.5, \lambda_R = 1$. We set $\lambda_S = 0$ for operations where no hair editing is done. The default value for Eq. (3) is set to $\epsilon = 0.05$. We again apply the Adam optimization algorithm [52] for the learning process. The learning rate is set to 0.001 for the latent code w and to 0.1 for the noise component n. Additional implementation details can be found in the publicly released implementation of MaskFaceGAN: https://github.com/MartinPernus/MaskFaceGAN.

C. Methods

MaskFaceGAN is evaluated in comparison with multiple competing face editing models, i.e., StarGAN [5], AttGAN [7], STGAN [8] and two versions of the InterFaceGAN framework [9], [14]. For a fair comparison, StarGAN, AttGAN and STGAN are trained on the same attributes as MaskFaceGAN (see Table I), using the models' official code repository[5]. We implement InterFaceGAN [9] on the StyleGAN2 latent space, following the linear SVM framework. In addition to the vanilla version of InterFaceGAN, the authors of [9] also introduced the concept of *conditional manipulation* that tries to disentangle facial attributes when editing facial images. We additionally consider such type of model in the experiments, where a single target attribute is manipulated at the time, while other attributes most entangled with the target one are excluded from the editing procedure. The original model is denoted as InterFaceGAN and its disentangled version as InterFaceGAN–D hereafter. Both of these models edit images by moving latent codes along attribute–dependent directions. The magnitude of this displacement is set to 1 based on preliminary experiments.

[4] Available from: https://github.com/NVlabs/stylegan2

[5] Available from: https://github.com/yunjey/stargan, https://github.com/LynnHo/AttGAN-Tensorflow, https://github.com/csmliu/STGAN, https://github.com/genforce/interfacegan

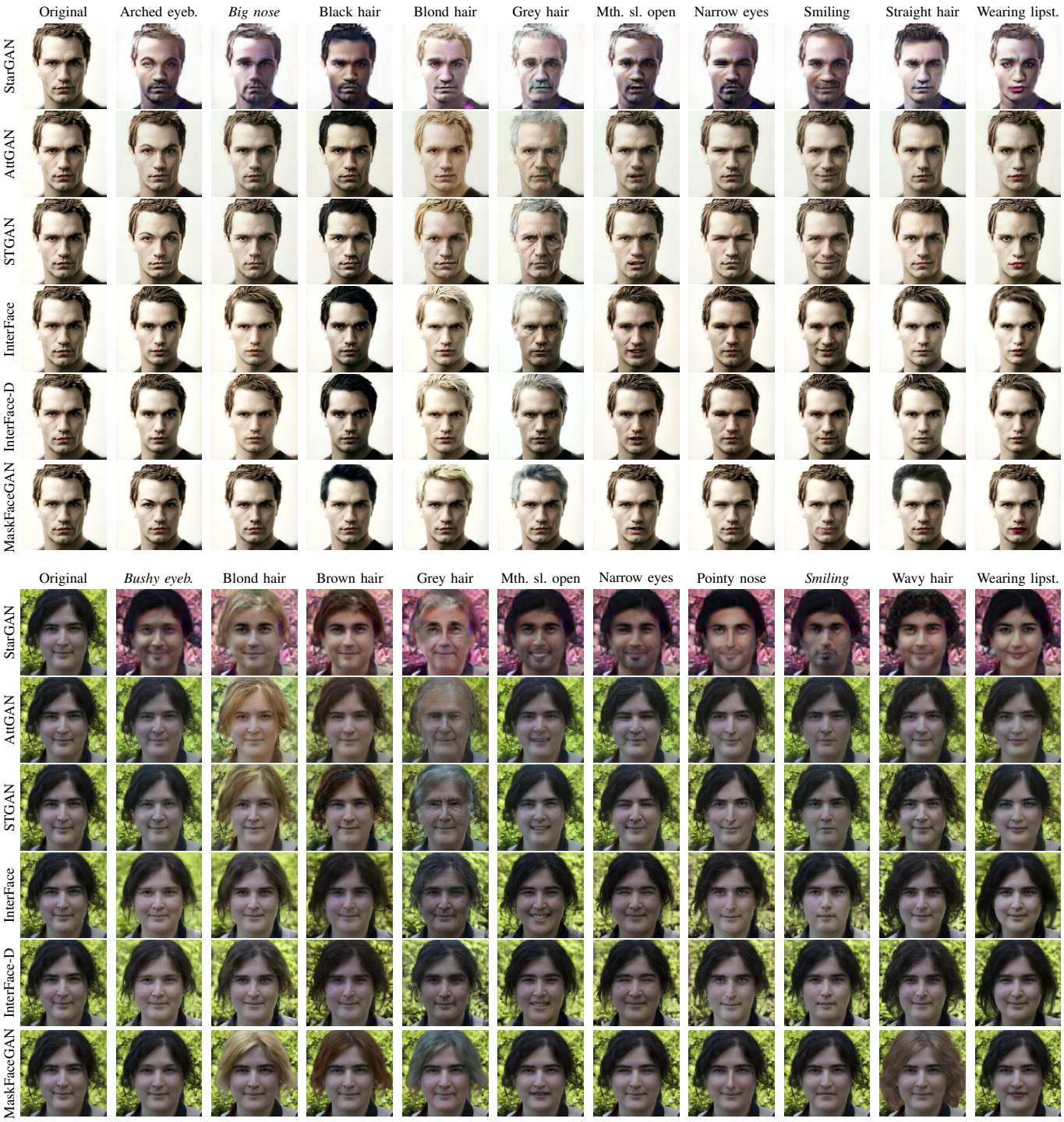

Fig. 5: Comparison of MaskFaceGAN and five state–of–the–art attribute editing models from the literature. Editing results are presented for 14 distinct facial attributes with spatial correspondences. For attributes already present in the image, editing inverts the result (e.g., removes the lipstick for "wearing lipstick" if it is already there) - displayed in italic. Results on the top correspond to a sample image from CelebA–HQ and results at the bottom to an image from Helen. Best viewed zoom in.

Note that the implemented models edit images at different resolutions, i.e., StarGAN produces edited images of 128×128 pixels, AttGAN and STGAN generate 384×384 images, while InterFaceGAN, InterFaceGAN–D and MaskFaceGAN edit images at a resolution of 1024×1024 pixels.

V. Results and Discussion

This section reports results that: (i) compare MaskFaceGAN to existing state–of–the–art attribute editing models, (ii) highlight some unique characteristics of the proposed approach, (iii) explore the contribution of various components through an ablation study, and (iv) investigate MaskFace-

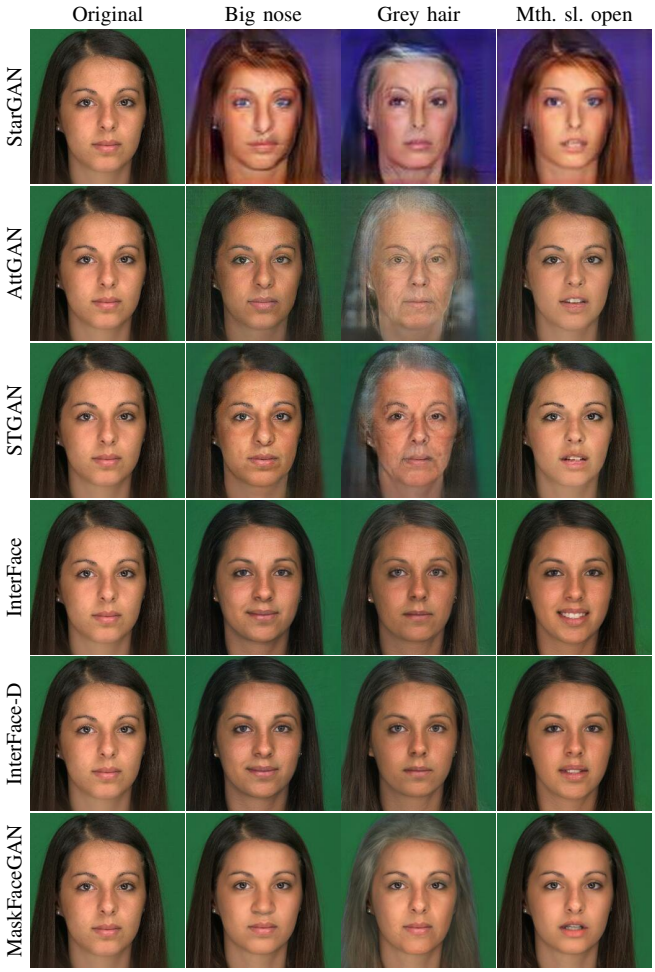

Fig. 6: Example results for a sample image from the SiblingsDB–HQf dataset. Editing examples are presented for three (often challenging) attributes in larger size to better highlight the difference in result quality. Note that especially for highly entangled attributes, such as "Grey hair", MaskFaceGAN ensures highly convincing results.

GAN's limitations.

A. Comparison to the State–Of–The–Art

Visual Analysis. We first demonstrate the performance of MaskFaceGAN for the task of single attribute editing and include the 14 binary attributes from Table I in the analysis. Three distinct datasets are used for the experiments to explore the generalization capabilities of the evaluated approaches across various data distributions. If a face already exhibits a given attribute (e.g., a face wearing lipstick), we generate edited faces with *inverted* attributes, (i.e., a face without lipstick).

Fig. 5 compares editing results produced by MaskFaceGAN and five competing models on a couple of sample images from the CelebA–HQ and Helen datasets. Note that 10 attributes are considered per example image to ensure a reasonable image size for the presentation. Among the encoder–decoder models, StarGAN generates the highest amount of visual artefacts and also introduces a background change for some of the attributes as illustrated with the sample image from Helen in Fig. 5. AttGAN and STGAN produce more convincing results, but still induce a certain amount of visual artefacts. These can, for example, be seen with the "Mouth slightly open" attribute in Fig. 5 and the editing results in Fig. 6, where higher–resolution edits for the SiblingsDB–HQf dataset are shown for three challenging (often entangled) attributes. The artefacts generated by the encoder-decoder methods stem from difficulties in balancing multiple loss terms commonly used when training such methods.

InterFaceGAN and InterFaceGAN–D are most closely related to MaskFaceGAN and achieve higher–quality editing result than the encoder–decoder models due to the use of the StyleGAN2 generator. The vanilla version of InterFaceGAN yields convincing target semantics, but due to the information entanglement in the latent codes, often changes correlated attributes in the process. This is best seen with the "Grey hair" attribute in Figs. 5 and 6, where the edited faces appear much older than the originals. InterFaceGAN–D is able to remove some of this disentaglement, but this requires a manual analysis of attribute correlations to exclude unwanted facial semantics from the editing procedure. We also observe a interesting behavior with the InterFaceGAN models, in that the same hyper–parameter setting (i.e., the magnitude of the latent code movement), results in attribute changes of different intensity for images of different characteristics – see, for example, the "Blond hair" results in Fig. 5 or "Grey hair" results in Figs. 5 and 6.

Compared to the competing models, the proposed MaskFaceGAN approach: (i) exhibits better disentanglement characteristics due to the latent space optimization procedure, which relies on attribute and spatial constraints, (ii) ensures artefact–free high–resolution attribute editing with convincing

TABLE III: FID scores produced by the evaluated editing models on the three experimental datasets (lower is better).

Method	CelebA–HQ	Helen	SiblingsDB–HQf
StarGAN [5]	140.87	152.64	176.84
AttGAN [7]	67.55	79.90	81.34
STGAN [8]	49.53	57.44	48.88
InterFaceGAN [9], [14]	79.79	90.93	83.40
InterFaceGAN–D [9], [14]	76.87	90.90	81.57
MaskFaceGAN (ours)	**32.56**	**34.00**	**34.53**

TABLE IV: User study results, where human raters were shown editing results of all tested models and asked to select the best one. Reported is the fraction of times [in %] a model was chosen as the overall best for a given dataset (higher is better).

Method	CelebA–HQ	Helen	SiblingsDB–HQf
StarGAN [5]	2.96%	2.76%	4.26%
AttGAN [7]	4.95%	6.53%	6.38%
STGAN [8]	13.93%	8.70%	12.60%
InterFaceGAN [9], [14]	7.49%	18.62%	18.80%
InterFaceGAN–D [9], [14]	9.99%	14.71%	10.82%
MaskFaceGAN (ours)	**60.68%**	**48.68%**	**47.14%**

TABLE V: User study results, where human raters were asked to rate the quality of the edited images on a 5–point Lickert scale (higher is better). Reported is the average score and corresponding standard deviation.

Method	CelebA–HQ	Helen	SiblingsDB–HQf
StarGAN [5]	1.46 ± 0.92	1.30 ± 0.63	1.52 ± 0.89
AttGAN [7]	2.85 ± 1.01	2.39 ± 1.06	2.48 ± 0.90
STGAN [8]	3.07 ± 1.13	2.44 ± 1.12	2.66 ± 0.98
InterFaceGAN [9], [14]	3.00 ± 1.03	3.03 ± 1.18	3.29 ± 1.02
InterFaceGAN–D [9], [14]	2.94 ± 1.12	2.78 ± 1.22	3.12 ± 1.10
MaskFaceGAN (ours)	$\mathbf{4.07 \pm 1.21}$	$\mathbf{3.80 \pm 1.23}$	$\mathbf{3.85 \pm 1.15}$

Original image | + Narrow eyes | + Narrow eyes + Blond hair | + Narrow eyes + Blond hair - Bushy eyebrows

Fig. 7: Editing multiple attributes with MaskFaceGAN. Every image is the result of a separate optimization procedure and is generated independently from all others.

image semantics, (iii) preserves important image details (e.g., facial areas not related to the target attribute or background), and (iv) does not require manual hyper–parameter tuning for each probe image separately.

Quantitative evaluation. To evaluate attribute editing performance in a quantitative manner, prior works [7], [8] reported a measure quantifying attribute generation accuracy. Because MaskFaceGAN tries to maximize this exact measure during latent code optimization, we use an alternative approach to ensure a fair comparison. Specifically, we first report Fréchet Inception Distances (FID) to quantify performance and then present results of a user study, similarly to [8].

- **FID Score Analysis.** The Fréchet Inception Distance (FID) [53] represents a common measure of image quality, predominantly used in the evaluation of GANs. It is defined as a measure between two Gaussian distributions of InceptionV3 image features, where the first distribution is calculated from the real data and the second is calculated from the generated data. We compute FID scores for each dataset considered in our evalution by first generating attribute specific FID scores and then averaging over all attributes. The facial images are rescaled to 299×299 pixels before extracting features. Table III shows that MaskFaceGAN achieves the lowest FID scores on all three test datasets, significantly outperforming all five competing editing models. The lower scores can mostly be attributed to the high quality of the edited images and lack of artefacts, which are the result of spatially constrained image modifications that only alter a small portion of the image for a given target attribute, while keeping other parts of the images intact.
- **User Study.** Following [8], we conduct a user study using a crowdsourcing platform to analyze the quality of the edited images. Here, the users (raters) were shown edited images of all considered models and asked to select the most convincing one based on the following instructions: *"Choose the image that changes the attribute more successfully, is of higher image quality and better preserves the identity and fine details of the source image."*. Additionally, they were also instructed to rate images on a

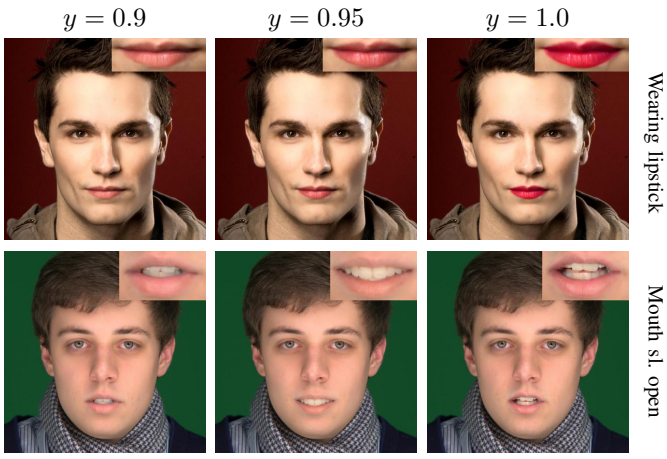

Fig. 8: Attribute intensity control. By varying the target probability $y = 1 - \epsilon$, MaskFaceGAN can achieve different intensities in the targeted attributes. A target probability of $y = 1.0$ creates an edited image that exhibits the most appropriate semantics according to the attribute classifier (C). Decreasing this probability lowers the attribute intensity.

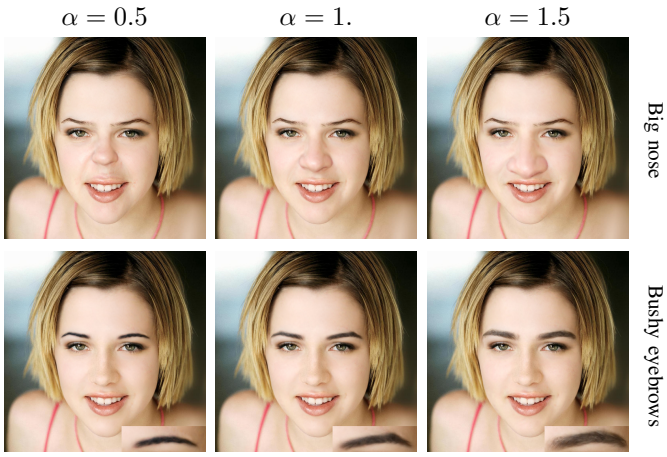

Fig. 9: Component size manipulation. By including an additional loss term (given in Eq. (6)), MaskFaceGAN can define the size of the image region to be edited. Setting $\alpha = 1$ preserves the original attribute size, while a setup of $\alpha < 1$ and $\alpha > 1$ reduces or enlarges the region size, respectively.

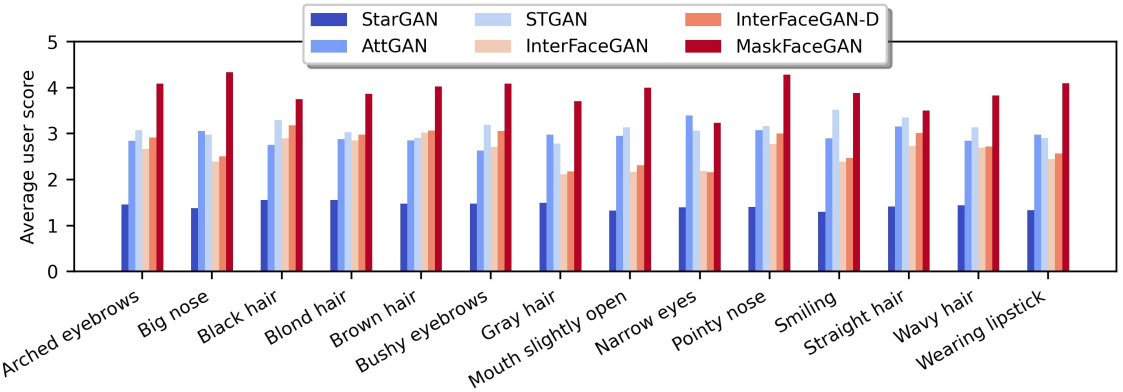

Fig. 10: Comparison of user study scores, averaged across all three dataset for individual attributes. As can be seen, MaskFaceGAN achieves highly competitive results with all targeted attributes. The figure is best viewed in color.

5–point Likert scale, where a higher number represents better image quality. A single user study covered all test images from a given dataset and was performed over all 14 attributes. Images were shown in random order for a fair comparison. The results, reported in Tables IV and V, show that MaskFaceGAN was most frequently selected as the best among the evaluated editing techniques and also received the highest average scores (on the 5–point Likert scale) on all three dataset. These observations are further supported by the results in Fig. 10, where user scores are reported for each edited attribute separately and MaskFaceGAN is again the top performer overall. The reported results speak of the excellent performance of MaskFaceGAN and competitiveness with respect to existing models.

B. Characteristics of MaskFaceGAN

MaskFaceGAN exhibits several desirable characteristics, such as the capability to (i) edit multiple attributes through at once, (ii) control the intensity of attribute editing, and (iii) modify the size of the edited region. Next, we illustrate these characteristics through several visual examples.

Multiple Attribute Editing. By averaging the KL divergence of the semantic content term over multiple attributes, MaskFaceGAN can edit multiple binary attributes through a single optimization procedure. Examples of such editing results are presented in Fig. 21 for different numbers of attributes, i.e., $K = \{1, 2, 3\}$. The optimization is always initialized with $(w', n') = (\bar{w}, 0)$. Two interesting observations can be made here: (i) even when multiple attributes are edited, the results are still visually convincing and artefact–free, and (ii) the joint optimization of several attributes retains considerable correspondence with the original image.

Attribute Intensity Control. The semantic content term used in MaskFaceGAN is defined by the KL divergence between the predictions of the attribute classifier (C) and the corresponding ground truth. Because the ground truth is smoothed and for the given attribute consists of $y \in \{\epsilon, 1-\epsilon\}$, varying the smoothing parameter ϵ affects the strength (or intensity) of the targeted attribute in the edited images.

A few illustrative examples of the impact of ϵ are presented in Fig. 8. Here, we edit the "Wearing lipstick" and "Mouth slightly open" attributes, but the same concept can also be applied to any of the remaining attributes. The presented examples show that MaskFaceGAN allows for control of the attribute intensity in the edited images, although the generated variations may not necessarily be smooth with respect to the visual appearance change. For example, the intensity change for the "Mouth slightly open" attribute in the bottom row of Fig. 8 does not simply open the mouth more, it can actually turn into a half–smile. The results primarily depend on the trained classifier and what it considers an attribute presence with $1 - \epsilon$ probability.

Component Size Manipulation. MaskFaceGAN can be adapted to include additional constraints. An example constraint is the desired size of the face component being manipulated. This is done by including the size manipulation loss term from Eq. (6) in the overall optimization objective in Eq. (9). In Fig. 9 we display results when specifying the portions of the original component size for $\alpha = \{0.5, 1.0, 1.5\}$. The results exhibit convincing component size manipulation performance, where the final attribute size corresponds to the specified component size.

Combining Editing Constraints. Multiple attribute editing, intensity control and component size manipulation can also be used simultaneously to change several aspects of the input face image with a single application of MaskFaceGAN. Fig. 11 presents an example of such an editing operation, where various aspects of the "Wearing lipstick" and "Bushy eyebrows" attributes are manipulated. Note that despite considerable changes to different facial attributes, the results still appear visually convincing.

C. Ablation Study

To demonstrate the impact of different component of MaskFaceGAN on the editing quality, we perform an ablation study on the CelebA–HQ dataset. Specifically, we focus on two major components of the proposed framework: (i) the shape term from Eq. (4), and (ii) the noise optimization procedure.

Fig. 11: An example of simultaneous component size manipulation and attribute intensity control. The attribute intensity is controlled by ϵ and the size of the edited component is controlled by parameter α. Results are shown for editing either a single (i.e., "Wearing lipstick") or two attributes (i.e., "Wearing lipstick" and "Bushy eyebrows") at the same time.

We note that the shape term only affects the hair region and does not impact other attributes.

Qualitative Analysis. Fig. 12 demonstrates the effect of different MaskFaceGAN settings. When the noise component is not optimized ($n = 0$), the edited images contain low frequency image areas, which is most apparent in the hair region, as shown in the second column of Fig. 12. Furthermore, the skin region is without certain details, e.g., beauty marks. The noise optimization ensures that such facial details and other high frequency components are present in the image – see third column of Fig. 12.

The absence of the shape term ($\lambda_S = 0$) results in suboptimal blending when dealing with hair modifications. In such settings, the background inpainted by the generator (G) is blended with the original background, resulting in unconvincing results with visible artefacts. The optimization of this term assures that the generator model gets information about the shape of the hair region during the inpainting step and produces photo realistic editing outputs.

Quantitative Analysis. For a quantitative analysis of the ablation results, we report in Table VIII mean FID scores computed over the test images of CelebA–HQ dataset and averaged over all attributes. Interestingly, the largest gain is obtained by the noise optimization procedure. Enabling the shape term to ensure blending conssitency results in additional FID gains. We hypothesize that these gains are a consequence of visually more convincing images, as shown in Fig. 12

D. Limitations

The results presented so far show that MaskFaceGAN generates competitive (high–quality) editing results when compared to state–of–the–art models from the literature. Nevertheless, the approach still exhibits a number of limitations.

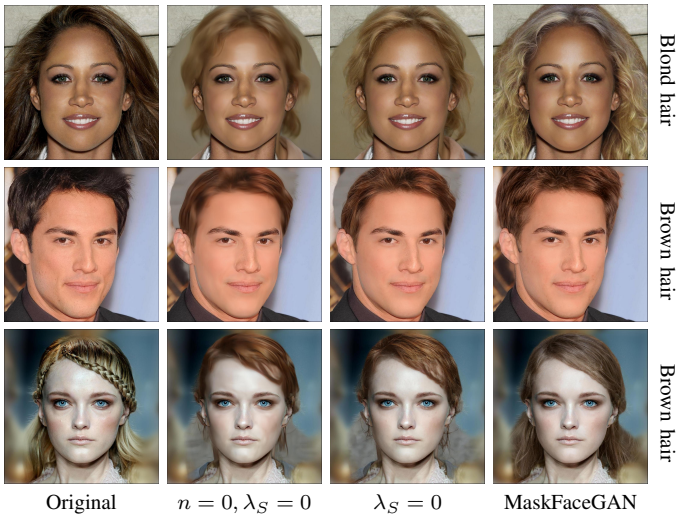

Fig. 12: Qualitative results of ablation study. The first column shows original images. The second column shows results without noise optimization and without considering the shape term. The third column illustrates the effect of the noise optimization - the images are sharper, particularly in the hair region. The last column shows results with the shape term enabled – the hair shape is consistent with the original images.

TABLE VI: Quantitative results of ablation study. FID scores computed on the CelebA–HQ dataset averaged over all attributes are reported (lower is better). Note that all components of MaskFaceGAN are important for the final performance.

MaskFaceGAN variant	FID
Local latent code optimization, no shape term	59.90
+ noise optimization	34.86
+ shape term (complete MaskFaceGAN)	**32.56**

MaskFaceGAN is based on gradient optimization that takes between 2 and 5 minutes per image on a GeForce GTX 1080. In comparison with encoder–decoder methods, that are capable of editing images in milliseconds, the proposed approach is slower by orders of magnitude. However, when compared to related embedding methods, e.g., Image2StyleGAN [15], [16], our local embedding procedure requires considerably fewer steps to converge.

The MaskFaceGAN framework relies on an attribute classifier (C) that steers the editing process. While this is an effective way of controlling the presence or absence of the targeted attribute in the edited image, it may produce inconsistent results for certain attributes. Our user study showed (see Fig. 10) that especially for the "Narrow eyes" attribute MaskFaceGAN does not convincingly outperform STGAN and AttGAN in terms of user scores. An analysis of this observation showed that MaskFaceGAN exhibits a tendency to close the eyes instead of trying to narrow the eyes to achieve the desired image manipulation, as illustrated in the first column of Fig. 13. While the edited image still looks convincing, such inconsistencies represents one of the limitations of MaskFaceGAN.

The second source of errors in the proposed framework is

+ Narrow eyes – *Smiling* + *Straight hair*

Fig. 13: Examples of MaskFaceGAN limitations. The original input images on the top are edited according to the listed target attributes. MaskFaceGAN is affected by the performance of the attribute classifier (C) and the face parser (S). Difficulties with these components are reflected in the editing results.

the face parser (S). For images, where S produces incorrect parsing results, the editing procedure operates with inappropriate spatial constraints and results in image changes in incorrect (or partially incorrect) regions. A couple of examples of such editing results are presented in the second and third column of Fig. 13, where the "Smiling" and "Straigth hair" attributes were used as the target for editing. Such limitations of MaskFaceGAN are expected to be mitigated with future advances in face parsing, as the parser used in this work can easily be replaced by a more advanced one.

VI. Conclusion

In this paper, we introduced MaskFaceGAN, a novel approach to high–resolution face image editing. At the core of the approach is a GAN latent code optimization procedure that generates targeted image regions in accordance with spatial and semantic constraints, enforced by pre–trained face parsing and classification networks. Through rigorous experiments on three public face datasetes, MaskFaceGAN was shown to convincingly alter a wide variety of facial attributes and ensure highly competitive performance when compared to state–of–the–art editing models from the literature. Additionally, the approach was demonstrated to enable unique editing characteristics, including attribute intensity control and component size manipulation.

As part of our future work, we plan to explore the use of latent code optimization strategies for face video editing, where the current bottleneck is the optimization speed. Encoder–based latent–space projections that allow to translate the existing MaskFaceGAN concepts to faster optimization procedures will be primarily considered for this work.

Acknowledgment

Supported by the ARRS Project J2-2501, the Research Programme P2-0250(B) and the ARRS junior researcher program.

References

[1] R. Tolosana, R. Vera-Rodriguez, J. Fierrez, A. Morales, and J. Ortega-Garcia, "Deepfakes and beyond: A survey of face manipulation and fake detection," *Information Fusion*, vol. 64, pp. 131–148, 2020.

[2] S. Jiang, Z. Tao, and Y. Fu, "Geometrically editable face image translation with adversarial networks," *IEEE Transactions on Image Processing*, vol. 30, pp. 2771–2783, 2021.

[3] V. Mirjalili, S. Raschka, and A. Ross, "Privacynet: semi-adversarial networks for multi-attribute face privacy," *IEEE Transactions on Image Processing*, vol. 29, pp. 9400–9412, 2020.

[4] H. Deng, C. Han, H. Cai, G. Han, and S. He, "Spatially-invariant style-codes controlled makeup transfer," in *Computer Vision and Pattern Recognition (CVPR)*, 2021, pp. 6549–6557.

[5] Y. Choi, M. Choi, M. Kim, J.-W. Ha, S. Kim, and J. Choo, "Stargan: Unified generative adversarial networks for multi-domain image-to-image translation," in *Computer Vision and Pattern Recognition (CVPR)*, 2018, pp. 8789–8797.

[6] Y. Jo and J. Park, "Sc-fegan: Face editing generative adversarial network with user's sketch and color," in *International Conference on Computer Vision (ICCV)*, 2019, pp. 1745–1753.

[7] Z. He, W. Zuo, M. Kan, S. Shan, and X. Chen, "Attgan: Facial attribute editing by only changing what you want," *IEEE Transactions on Image Processing*, vol. 28, no. 11, pp. 5464–5478, 2019.

[8] M. Liu, Y. Ding, M. Xia, X. Liu, E. Ding, W. Zuo, and S. Wen, "Stgan: A unified selective transfer network for arbitrary image attribute editing," in *Computer Vision and Pattern Recognition (CVPR)*, 2019, pp. 3673–3682.

[9] Y. Shen, J. Gu, X. Tang, and B. Zhou, "Interpreting the latent space of gans for semantic face editing," in *Computer Vision and Pattern Recognition (CVPR)*, 2020, pp. 9243–9252.

[10] I. Goodfellow, J. Pouget-Abadie, M. Mirza, B. Xu, D. Warde-Farley, S. Ozair, A. Courville, and Y. Bengio, "Generative adversarial nets," in *Advances in neural information processing systems (NIPS)*, 2014, pp. 2672–2680.

[11] Z. Shu, E. Yumer, S. Hadap, K. Sunkavalli, E. Shechtman, and D. Samaras, "Neural face editing with intrinsic image disentangling," in *Computer Vision and Pattern Recognition (CVPR)*, 2017, pp. 5541–5550.

[12] S. Sengupta, A. Kanazawa, C. D. Castillo, and D. W. Jacobs, "Sfsnet: Learning shape, reflectance and illuminance of faces in the wild," in *Computer Vision and Pattern Recognition (CVPR)*, 2018, pp. 6296–6305.

[13] W. Xia, Y. Zhang, Y. Yang, J.-H. Xue, B. Zhou, and M.-H. Yang, "GAN Inversion: A Survey," *arXiv preprint arXiv:2101.05278*, 2021.

[14] Y. Shen, C. Yang, X. Tang, and B. Zhou, "Interfacegan: Interpreting the disentangled face representation learned by gans," *IEEE Transactions on Pattern Analysis and Machine Intelligence*, 2021.

[15] R. Abdal, Y. Qin, and P. Wonka, "Image2stylegan: How to embed images into the stylegan latent space?" in *International Conference on Computer Vision (ICCV)*, 2019, pp. 4431–4440.

[16] ——, "Image2stylegan++: How to edit the embedded images?" in *Computer Vision and Pattern Recognition (CVPR)*, 2020, pp. 8296–8305.

[17] T. Karras, S. Laine, M. Aittala, J. Hellsten, J. Lehtinen, and T. Aila, "Analyzing and improving the image quality of stylegan," in *Computer Vision and Pattern Recognition (CVPR)*, 2020, pp. 8110–8119.

[18] H. Zhang, I. Goodfellow, D. Metaxas, and A. Odena, "Self-attention generative adversarial networks," in *International Conference on Machine Learning (ICML)*, 2019, pp. 7354–7363.

[19] A. Brock, J. Donahue, and K. Simonyan, "Large scale gan training for high fidelity natural image synthesis," in *International Conference on Learning Representations (ICLR)*, 2018.

[20] J. Johnson, A. Gupta, and L. Fei-Fei, "Image generation from scene graphs," in *Computer Vision and Pattern Recognition (CVPR)*, 2018, pp. 1219–1228.

[21] O. Ashual and L. Wolf, "Specifying object attributes and relations in interactive scene generation," in *International Conference on Computer Vision (ICCV)*, 2019, pp. 4561–4569.

[22] T. Park, M.-Y. Liu, T.-C. Wang, and J.-Y. Zhu, "Semantic image synthesis with spatially-adaptive normalization," in *Computer Vision and Pattern Recognition (CVPR)*, 2019, pp. 2337–2346.

[23] T. Xu, P. Zhang, Q. Huang, H. Zhang, Z. Gan, X. Huang, and X. He, "Attngan: Fine-grained text to image generation with attentional generative adversarial networks," in *Computer Vision and Pattern Recognition (CVPR)*, 2018, pp. 1316–1324.

[24] H. Tan, X. Liu, M. Liu, B. Yin, and X. Li, "Kt-gan: Knowledge-transfer generative adversarial network for text-to-image synthesis," *IEEE Transactions on Image Processing*, vol. 30, pp. 1275–1290, 2021.
[25] Y. Yang, L. Wang, D. Xie, C. Deng, and D. Tao, "Multi-sentence auxiliary adversarial networks for fine-grained text-to-image synthesis," *IEEE Transactions on Image Processing*, vol. 30, pp. 2798–2809, 2021.
[26] A. Radford, L. Metz, and S. Chintala, "Unsupervised representation learning with deep convolutional generative adversarial networks," in *International Conference on Learning Representations (ICLR)*, 2016.
[27] T. Karras, T. Aila, S. Laine, and J. Lehtinen, "Progressive growing of gans for improved quality, stability, and variation," in *International Conference on Learning Representations (ICLR)*, 2018.
[28] T. Karras, S. Laine, and T. Aila, "A style-based generator architecture for generative adversarial networks," in *Computer Vision and Pattern Recognition (CVPR)*, 2019, pp. 4401–4410.
[29] X. Mao, Q. Li, H. Xie, R. Y. Lau, Z. Wang, and S. Paul Smolley, "Least squares generative adversarial networks," in *International Conference on Computer Vision (ICCV)*, 2017, pp. 2794–2802.
[30] M. Arjovsky, S. Chintala, and L. Bottou, "Wasserstein generative adversarial networks," in *International Conference on Machine Learning (ICML)*, 2017, pp. 214–223.
[31] I. Gulrajani, F. Ahmed, M. Arjovsky, V. Dumoulin, and A. C. Courville, "Improved training of wasserstein gans," in *Advances in Neural Information Processing Systems (NIPS)*, 2017, pp. 5767–5777.
[32] T. Miyato, T. Kataoka, M. Koyama, and Y. Yoshida, "Spectral normalization for generative adversarial networks," in *International Conference on Learning Representations (ICLR)*, 2018.
[33] L. Mescheder, A. Geiger, and S. Nowozin, "Which training methods for gans do actually converge?" in *International Conference on Machine learning (ICML)*, 2018, pp. 3481–3490.
[34] Z. Wang, Q. She, and T. E. Ward, "Generative adversarial networks in computer vision: A survey and taxonomy," *ACM Computing Surveys*, vol. 54, no. 2, pp. 1–38, 2021.
[35] D. Saxena and J. Cao, "Generative adversarial networks (gans) challenges, solutions, and future directions," *ACM Computing Surveys*, vol. 54, no. 3, pp. 1–42, 2021.
[36] D. Bau, J.-Y. Zhu, H. Strobelt, B. Zhou, J. B. Tenenbaum, W. T. Freeman, and A. Torralba, "Gan dissection: Visualizing and understanding generative adversarial networks," in *International Conference on Learning Representations (ICLR)*, 2019.
[37] A. Jahanian, L. Chai, and P. Isola, "On the" steerability" of generative adversarial networks," in *International Conference on Learning Representations (ICLR)*, 2020.
[38] L. Goetschalckx, A. Andonian, A. Oliva, and P. Isola, "Ganalyze: Toward visual definitions of cognitive image properties," in *International Conference on Computer Vision (ICCV)*, 2019, pp. 5744–5753.
[39] C. Yang, Y. Shen, and B. Zhou, "Semantic hierarchy emerges in deep generative representations for scene synthesis," *International Journal of Computer Vision*, pp. 1–16, 2021.
[40] J. Lin, R. Zhang, F. Ganz, S. Han, and J.-Y. Zhu, "Anycost gans for interactive image synthesis and editing," in *Computer Vision and Pattern Recognition (CVPR)*, 2021, pp. 14 986–14 996.
[41] M. Afifi, M. A. Brubaker, and M. S. Brown, "Histogan: Controlling colors of gan-generated and real images via color histograms," in *Computer Vision and Pattern Recognition (CVPR)*, 2021, pp. 7941–7950.
[42] T. Portenier, Q. Hu, A. Szabo, S. Arjomand, P. Favaro, and M. Zwicker, "Faceshop: Deep sketch-based image editing," *ACM transactions on graphics*, vol. 37, no. 4, pp. 1–13, 2018.
[43] C.-H. Lee, Z. Liu, L. Wu, and P. Luo, "Maskgan: Towards diverse and interactive facial image manipulation," in *Computer Vision and Pattern Recognition (CVPR)*, 2020, pp. 5549–5558.
[44] J.-Y. Zhu, T. Park, P. Isola, and A. A. Efros, "Unpaired image-to-image translation using cycle-consistent adversarial networks," in *International Conference on Computer Vision (ICCV)*, 2017, pp. 2223–2232.
[45] S. Vandenhende, S. Georgoulis, B. De Brabandere, and L. Van Gool, "Branched multi-task networks: deciding what layers to share," in *British Machine Vision Conference (BMVC)*, 2020.
[46] L.-C. Chen, G. Papandreou, F. Schroff, and H. Adam, "Rethinking atrous convolution for semantic image segmentation," in *Computer Vision and Pattern Recognition (CVPR)*, 2017.
[47] Z. Liu, P. Luo, X. Wang, and X. Tang, "Deep learning face attributes in the wild," in *International Conference on Computer Vision (ICCV)*, 2015, pp. 3730–3738.
[48] T. Van Erven and P. Harremos, "Rényi divergence and Kullback-Leibler divergence," *IEEE Transactions on Information Theory*, vol. 60, no. 7, pp. 3797–3820, 2014.
[49] V. Le, J. Brandt, Z. Lin, L. Bourdev, and T. S. Huang, "Interactive facial feature localization," in *European Conference on Computer Vision (ECCV)*, 2012, pp. 679–692.
[50] A. Vieira, Tiago F.and Bottino, A. Laurentini, and M. De Simone, "Detecting siblings in image pairs," *The Visual Computer*, vol. 30, no. 12, pp. 1333–1345, Dec 2014.
[51] I. Sutskever, J. Martens, G. Dahl, and G. Hinton, "On the importance of initialization and momentum in deep learning," in *International Conference on Machine Learning (ICML)*, 2013, pp. 1139–1147.
[52] D. P. Kingma and J. Ba, "Adam: A method for stochastic optimization," in *International Conference on Learning Representations (ICLR)*, 2014.
[53] M. Heusel, H. Ramsauer, T. Unterthiner, B. Nessler, and S. Hochreiter, "Gans trained by a two time-scale update rule converge to a local nash equilibrium," in *Advances in neural information processing systems (NIPS)*, 2017, pp. 6626–6637.
[54] R. Zhang, P. Isola, A. A. Efros, E. Shechtman, and O. Wang, "The unreasonable effectiveness of deep features as a perceptual metric," in *Computer Vision and Pattern Recognition (CVPR)*, 2018, pp. 586–595.
[55] J. Johnson, A. Alahi, and L. Fei-Fei, "Perceptual losses for real-time style transfer and super-resolution," in *European conference on computer vision*, 2016, pp. 694–711.
[56] A. Dosovitskiy and T. Brox, "Generating images with perceptual similarity metrics based on deep networks," *Advances in neural information processing systems*, vol. 29, pp. 658–666, 2016.
[57] R. R. Selvaraju, M. Cogswell, A. Das, R. Vedantam, D. Parikh, and D. Batra, "Grad-cam: Visual explanations from deep networks via gradient-based localization," in *Proceedings of the IEEE international conference on computer vision*, 2017, pp. 618–626.

MaskFaceGAN: High Resolution Face Editing with Masked GAN Latent Code Optimization – Supplementary Material

Martin Pernuš, *Student Member, IEEE,* Vitomir Štruc, *Senior Member, IEEE,* and Simon Dobrišek, *Member, IEEE*

***Abstract*—In the main part of the paper, we introduced the MaskFaceGAN face editing approach and presented several experiments to demonstrate its capabilities. This *Supplementary material* provides further details on MaskFaceGAN and reports additional results to highlight the merits of the proposed approach. Specifically, the supplementary material: (i) elaborates on the importance and effect of the local GAN inversion used by MaskFaceGAN, (ii) further motivates the use of spatial constraints for face attribute editing, (iii) presents additional editing results for all targeted attributes, (iv) investigates the editing quality at higher resolutions, (v) explores attribute intensity control and component size manipulation for additional attributes not considered in the main part of the paper, (vi) reports per–attribute results for the ablation study, FID analysis and user study, (vii) discusses details with respect to the implementation of the user study and the compared models included in the experimental evaluations.**

VII. Embedding quality and local GAN inversion

Unlike competing approaches to face attribute editing that rely on latent code optimization, e.g., [9], [15], [16], MaskFaceGAN does not embed the entire face image into the GAN latent space. Instead, it only embeds facial region(s) needed for editing, which results in higher quality embeddings. In the main part of paper, we showed a visual example to illustrate this characteristic. Here, we report results of a simple experiment aimed at evaluating image quality when embedding smaller image regions and blending the result with the rest of the original input image.

For the experiment, the target face region is embedded with a masked MSE loss. We optimize the latent code w for 2000 iterations, reconstruct the output image, blend it with the original and then report average PSNR, SSIM, MSE and perceptual loss (PL) (computed over conv1-conv5 features of the VGG ImageNet model as in [54]) scores computed over 10 randomly selected face images from CelebA–HQ. The results reported Table VII reflect the similarity between the blended and the original input image and (among others) serve as a indicators of the visual quality of the outputs of MaskFaceGAN. We note at this point that image manipulation techniques based on GAN inversion need to ensure that the edited images are as close to the original as possible and that important characteristics, such as the identity of the subject shown, the background and other semantically critical image aspects are captured by the embedding process.

Table VII shows the performance scores achieved by MaskFaceGAN, when embedding different (local) facial regions, and a comparison with the state–of–the–art Image2StyleGAN++ algorithm from [16]. For the latter the whole face is embedded in the latent space using a combination of pixel–wise MSE and perceptual losses [55], [56]. We observe that choosing to embed a smaller portion of the image results in a high gain of embedding quality. It is important to note that the results should not be regarded as an improvement over existing embedding algorithms – one could achieve a perfect score by simply choosing to embed no part of the image. Nevertheless, they motive the idea of focusing the editing procedure on local image areas. Because in the main part of the paper we report editing results on larger datasets than, for example, [16], this local embedding step allows us to perform a lower number of iterations during the optimization procedure and still generate visually convincing and photo–realistic images.

TABLE VII: Comparison of StyleGAN latent code embedding quality, where the quality is measured by the similarity of the image generated from the optimized latent code and the original input image. The arrows next to the performance scores indicate whether a higher (↑) or lower (↓) score corresponds to better performance.

Method	MSE $\cdot 10^4$ ↓	PSNR ↑	SSIM ↑	PL ↓
Image2StyleGAN++ [16]	89.9	20.87	0.81	0.23
MMSE – face	24.0	26.73	0.90	0.20
MMSE – no hair	8.0	31.01	0.97	0.06
MMSE – skin only	3.9	34.11	0.99	0.05

VIII. Spatial constraints and facial attribute correspondence

MaskFaceGAN relies on spatial constraints when optimizing StyleGAN2 the latent–codes for facial attribute editing. The edited attributes, therefore, need to have spatial correspondences and visually convincing changes in the attributes need to be reflected in local image regions only. To demonstrate that utilizing spatial constraints for image editing is reasonable, we visualize image areas contributing most to the decision of MaskFaceGANs attribute classifier C for a number of target attributes in Fig. 14. Here, GradCAM [57] is utilized to generate spatial heatmaps for the visualization.

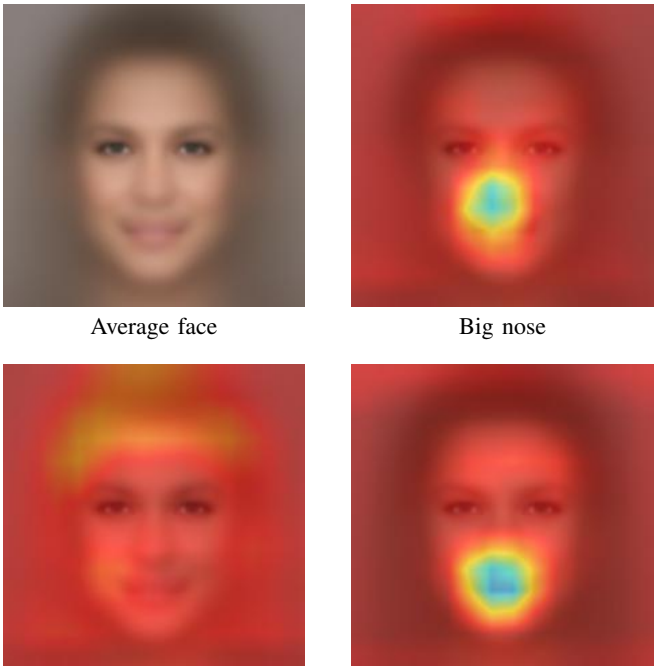

Fig. 14: Visualization of the image regions with the greatest impact on attribute classifier C for a given attribute. The heatmpas were generated with GradCAM. The left image in the top row shows the average CelebA–HQ face. The remaining images contain the average face overlayed with average GradCAM heatmaps for a few sample attributes. Note that the attributes are reflected in local image regions.

For this experiment, we extract heatmaps from a subset of images from CelebA–HQ. Due to the tree–like architecture of the classifier used in our implementation of MaskFaceGAN, only gradients and activations from the leaf convolutional layer of a given target facial attribute are considered. All other leaf convolutional layers do not receive any gradient and, therefore, have zero contribution to the heatmaps. In Fig. 14 the average CelebA–HQ face as well average GradCam heatmaps (computed over the subset of CelebA–HQ images) for a few example attributes are presented. Note that the classifier focuses predominantly on local image regions, suggesting that changing the image within a local image region is a viable approach for such attributes.

IX. Additional Editing Results

In this section, we present additional visual results for all targeted facial attributes and across images from all three experimental datasets.

A. Single Attribute Editing

Figs. 15, 16 and 17 show editing examples for images from CelebA–HQ, Helen and SiblingsDB–HQf, respectively. The StarGAN model shows a somewhat weaker performance than other editing techniques considered and exhibits limited generalization capabilities across different datasets, as shown in Figs. 16 and 17. AttGAN and STGAN produce higher–quality editing results, but often struggle with the entanglement of different attributes, which is especially apparent with the "Grey hair" attribute. The disentangled version of InterFaceGAN, InterFaceGAN–D, is more successful with entangled attributes. For example, it relatively convincingly removes age–dependent image characteristics, such as wrinkles, when trying to generate "Grey hair", as shown in Fig. 15. However, disentangling "Pale skin" from hair color does not have any apparent effect compared to the vanilla InterFaceGAN version, as shown in Fig. 15 under "Blond hair" and in Fig. 16 under "Black hair" despite the fact that these attributes are highly correlated. MaskFaceGAN, on the other hand, is less affected by disentaglement due to the local nature of the editing procedure and produces convincing results for the majority of edited attributes.

B. High Resolution Results

Fig. 18 presents high–resolution editing results for the "Blond hair" attribute. In this example, the StarGAN model produces the most blurry result due to the low image resolution of the model. AttGAN and STGAN achieve better image quality. However, the edited images still exhibit visual artefacts. For the presented results, InterFaceGAN–D is disentangled with respect to the "Pale skin" attribute. Nonetheless, both InterFaceGAN as well as its disentangled version InterFaceGAN–D edit the image with very similar results that slightly changes the skin tone as well as color and shape of clothes, background, ears and eye region. The proposed model does not exhibit such entangled properties and preserves both appearance as well as identity of the original face well. Additionally, even at higher resolutions, no apparent artefacts are present in the edited image.

C. Attribute Intensity Control

Fig. 19 shows editing results generated by varying the ϵ value to achieve different intensities of the attribute presence/absence in the edited image. Lowering the ϵ values towards 0 results in stronger semantic content (i.e., stronger presence) of the targeted attribute. As illustrated in Fig. 19, MaskFaceGAN enables a considerable level of control over the intensity of different facial attributes, such as hair color, eyebrow shape, smiling intensity and nose size. Note how all edited images appear photo realistic despite varying intensities of the targeted attributes.

D. Component Size Manipulation

Fig. 20 presents results that demonstrate MaskFaceGAN's ability to manipulate the size of the spatial region to be edited for a given target attribute. Specifically, the figure shows results for five targeted attributes and different scaling factors α, which defines the target attribute size with respect to the initial size of the region associated with a given attribute. Varying the scaling factor α allows MaskFaceGAN to grow or shrink certain face parts. Due to the shape term in the loss equation that assures consistent blending, we only allow

Fig. 15: Attributes editing examples for a sample image from the CelebA–HQ dataset. The results show manipulation of a single attribute and a comparison to the results generated with competing models. Inverted attributes are marked italic. The figure is best viewed electronically and zoomed in for details.

Fig. 16: Attributes editing examples for a sample image from the Helen dataset. The results show manipulation of a single attribute and a comparison to the results generated with competing models. Inverted attributes are marked italic. The figure is best viewed electronically and zoomed in for details.

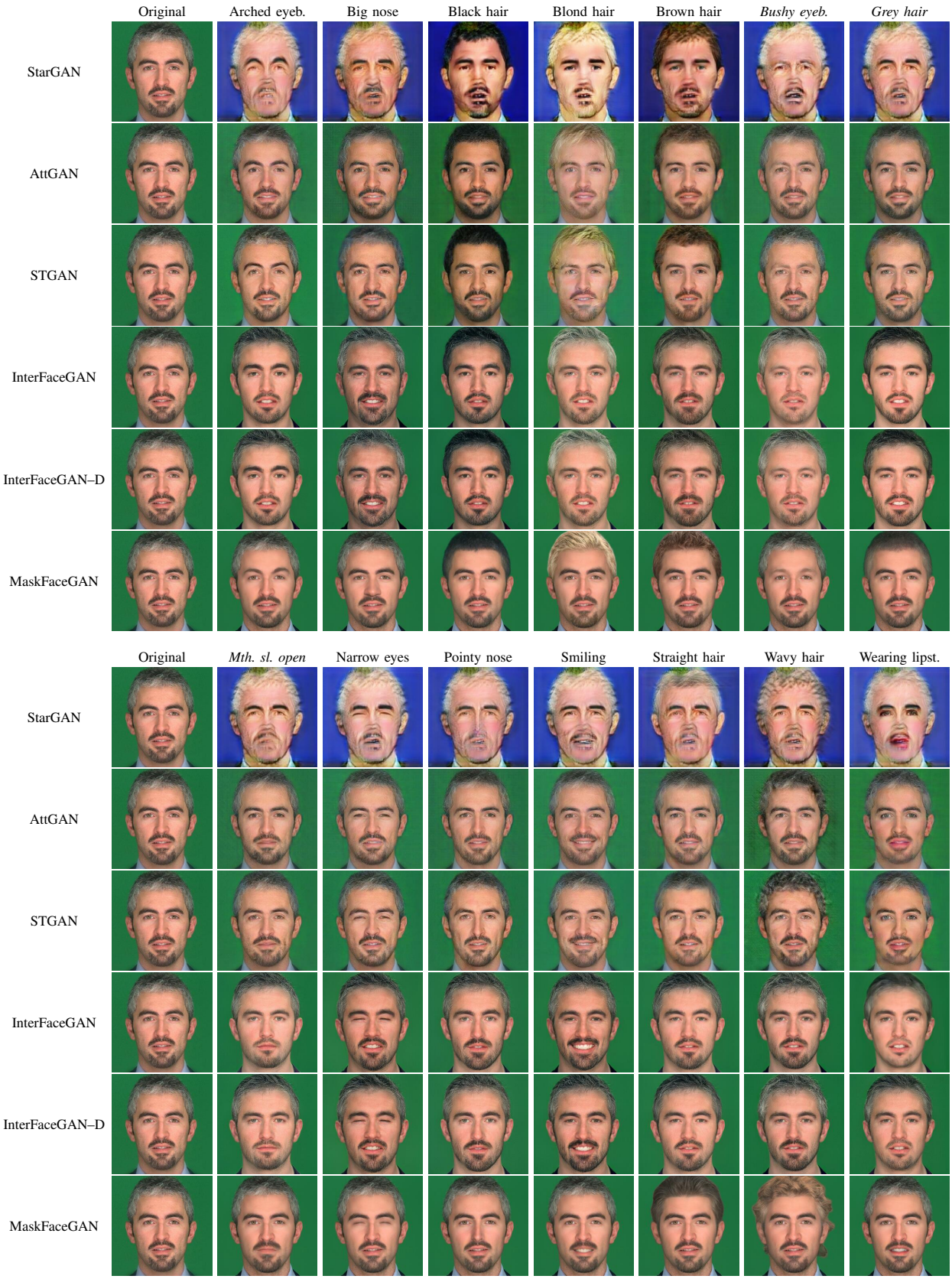

Fig. 17: Attributes editing examples for a sample image from the SiblingsDB–HQf dataset. The results show manipulation of a single attribute and a comparison to the results generated with competing models. Inverted attributes are marked italic. The figure is best viewed electronically and zoomed in for details.

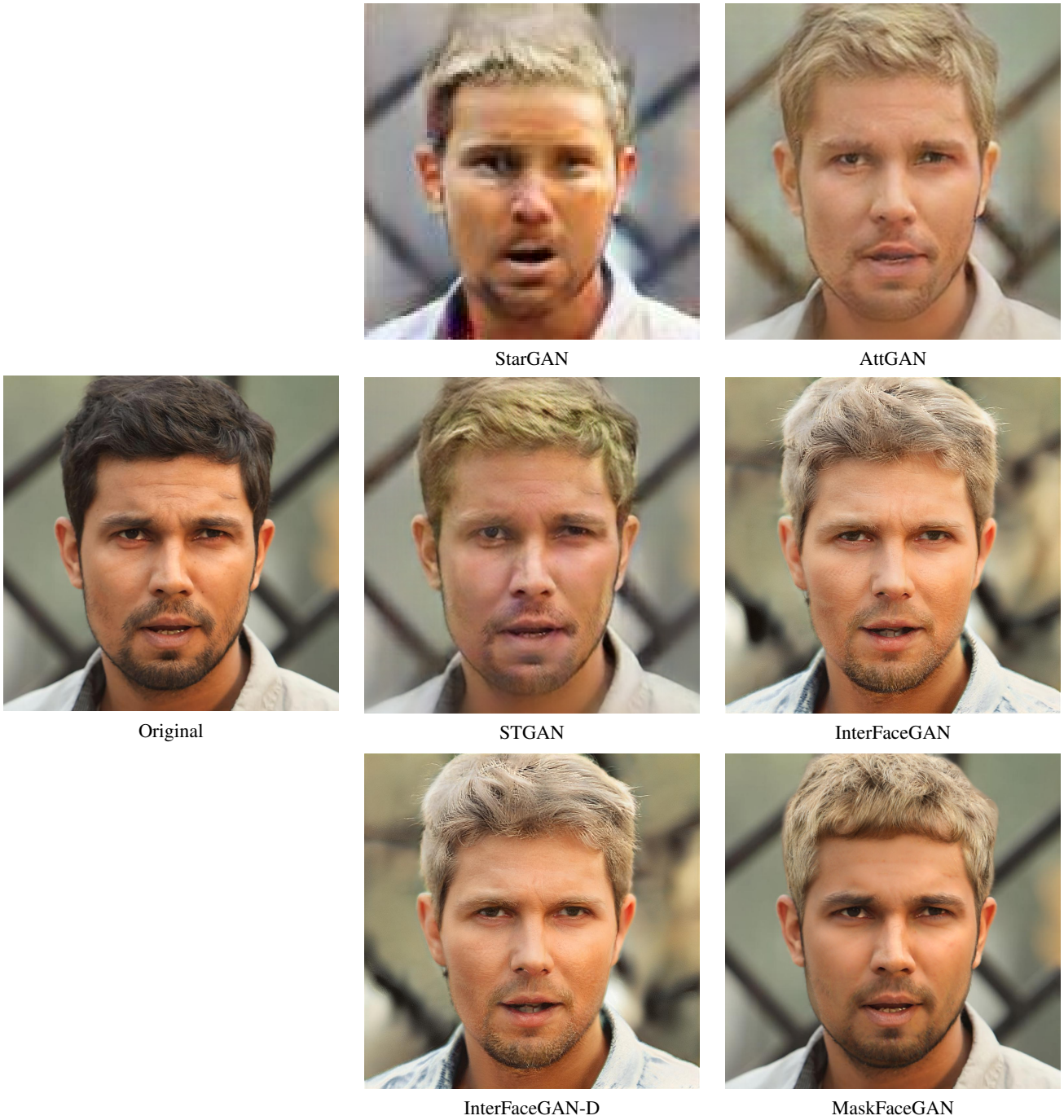

Fig. 18: High–resolution comparison of the proposed MaskFaceGAN approach and several state of the art editing techniques from the literature for the target attribute "Blond hair". Observe the quality of the generated images (the right two columns) and the details retained from the original input image on the left. While some of the competing models ensure solid results, MaskFaceGAN produces the most convincing image manipulations with the least amount of visible artefacts.

growing of hair (not shrinking). Other face components, such as the nose, eyebrows or mouth, on the other hand, can be shrunk as well. As can be seen from the presented examples, the ability of MaskFaceGAN to control the size of the spatial region during editing enables diverse image manipulations around the same targeted attribute and represents a unique feature of the proposed editing procedure.

E. Multiple Attribute Editing

Fig. 21 presents visual results when editing multiple attributes with a single optimization procedure. We show example for jointly editing two attribute but our experiments suggest

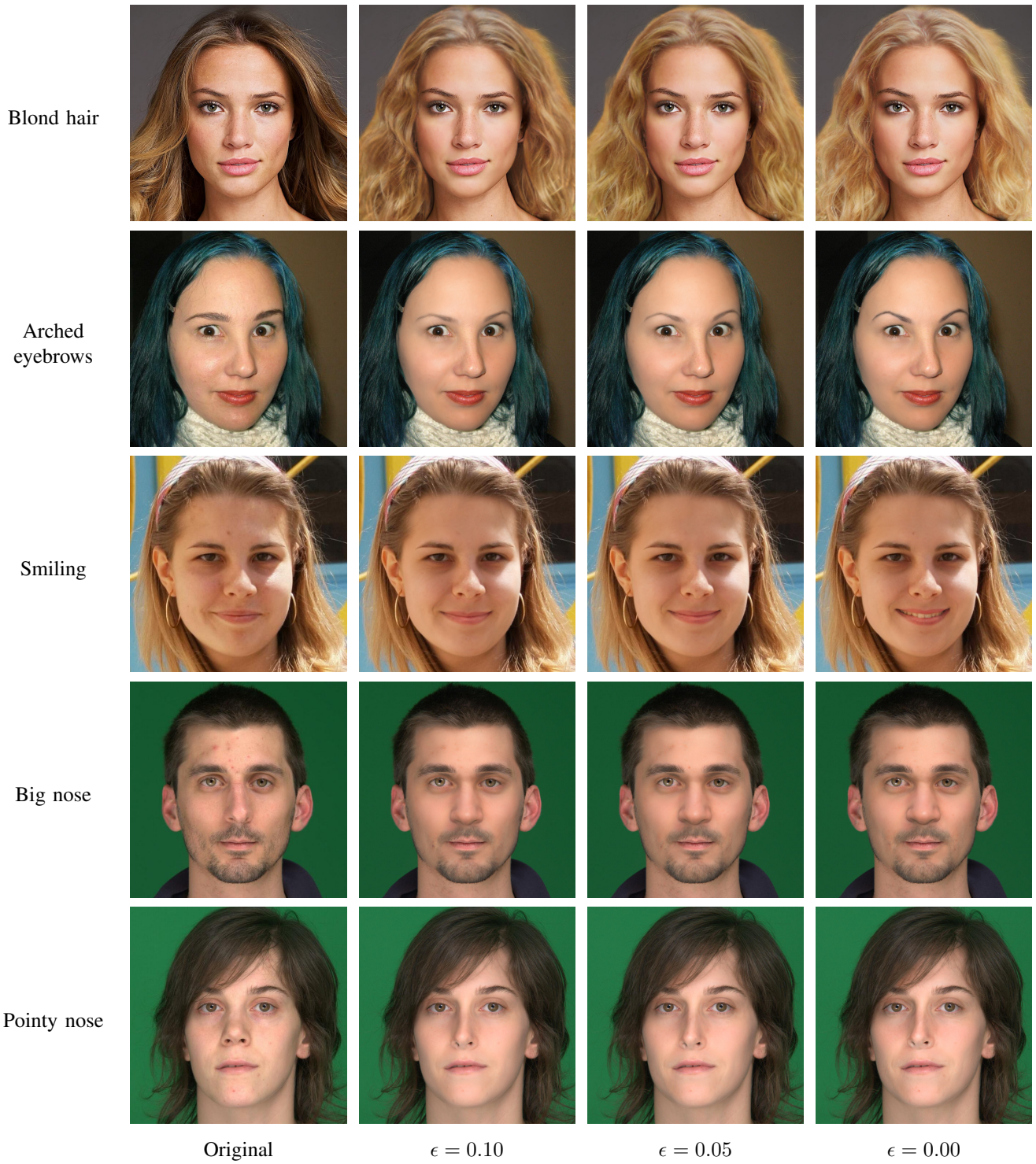

Fig. 19: Examples of intensity control for various smoothing ϵ values. MaskFaceGAN allows for fine grained control over attribute appearance despite being trained with binary attribute labels. Intensity control can be applied to a wide variety of facial attributes that affect color, shape or even more complex changes of facial appearance.

that realistic results are generated even if more attributes are considered. As illustrated in Fig. 21, the editing procedure can also *target the same facial components/region* even if multiple attributes are edited at the same time – see the (*Wearing lipst.*, Mouth sl. open), (Bushy eyeb., Arched eyeb.), (*Smiling*, *Wearing lipst.*) and (Smiling, Mouth sl. open) results. Despite having to accomodate different target semantics in the same spatial region, MaskFaceGAN generates realistic facial appearances and produces virtually no visual artefacts.

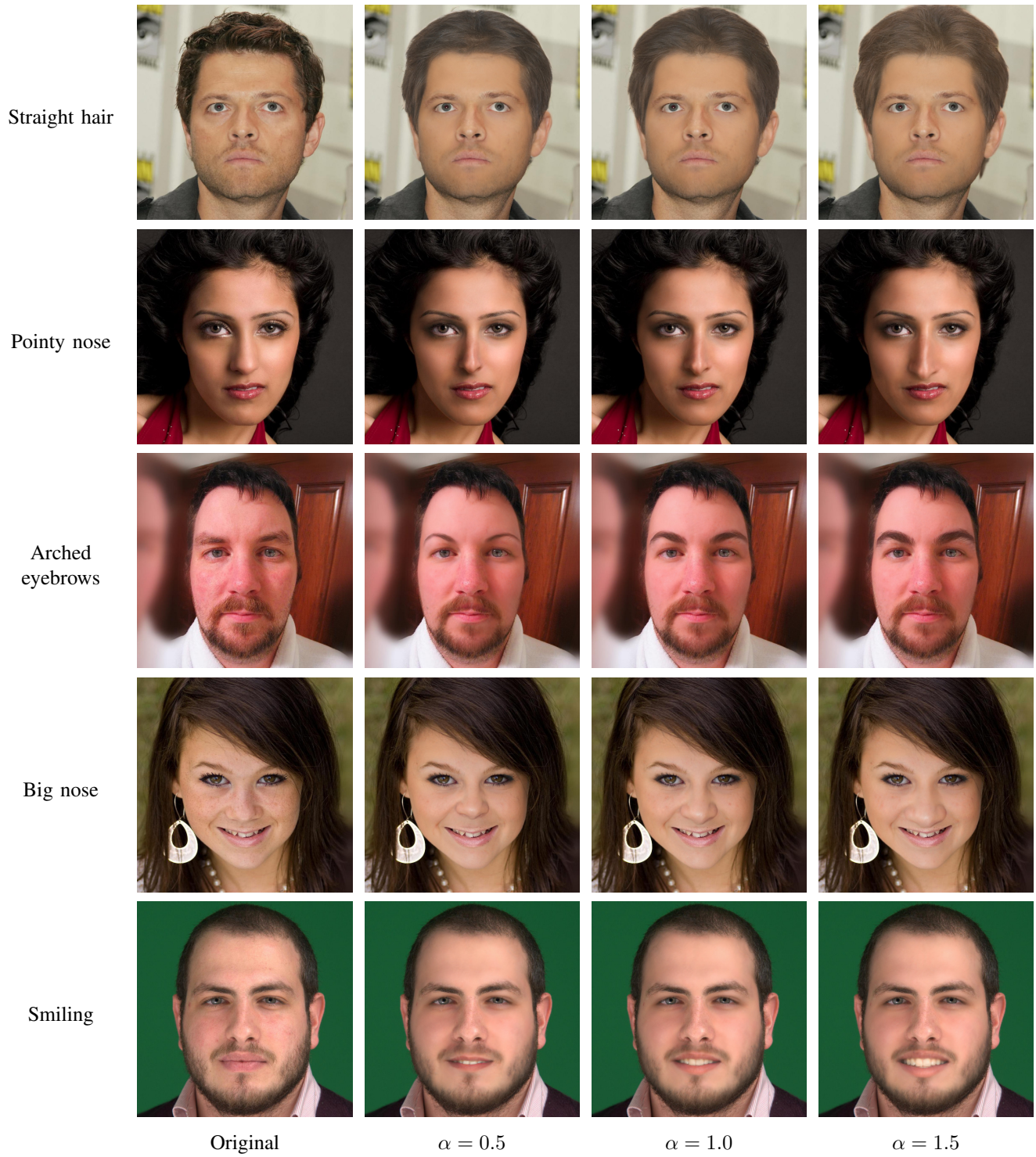

Fig. 20: Examples of component size manipulation for various scaling factors α. MaskFaceGAN allows growing the spatial region within which a targeted attribute is edited. This results in flexible image editing that can generate images with different versions of a targeted attribute in terms of size.

X. Results by Attributes

Next, we show quantitative results grouped by attributes. We analyze FID scores and user–study ratings.

A. Ablation Study

To ensure better insight into the contribution of individual components on the performance MaskFaceGAN, we again remove the noise optimization procedure and shape terms from our model investigate the impact of these components on the FID scores generated per attribute on the three experimental

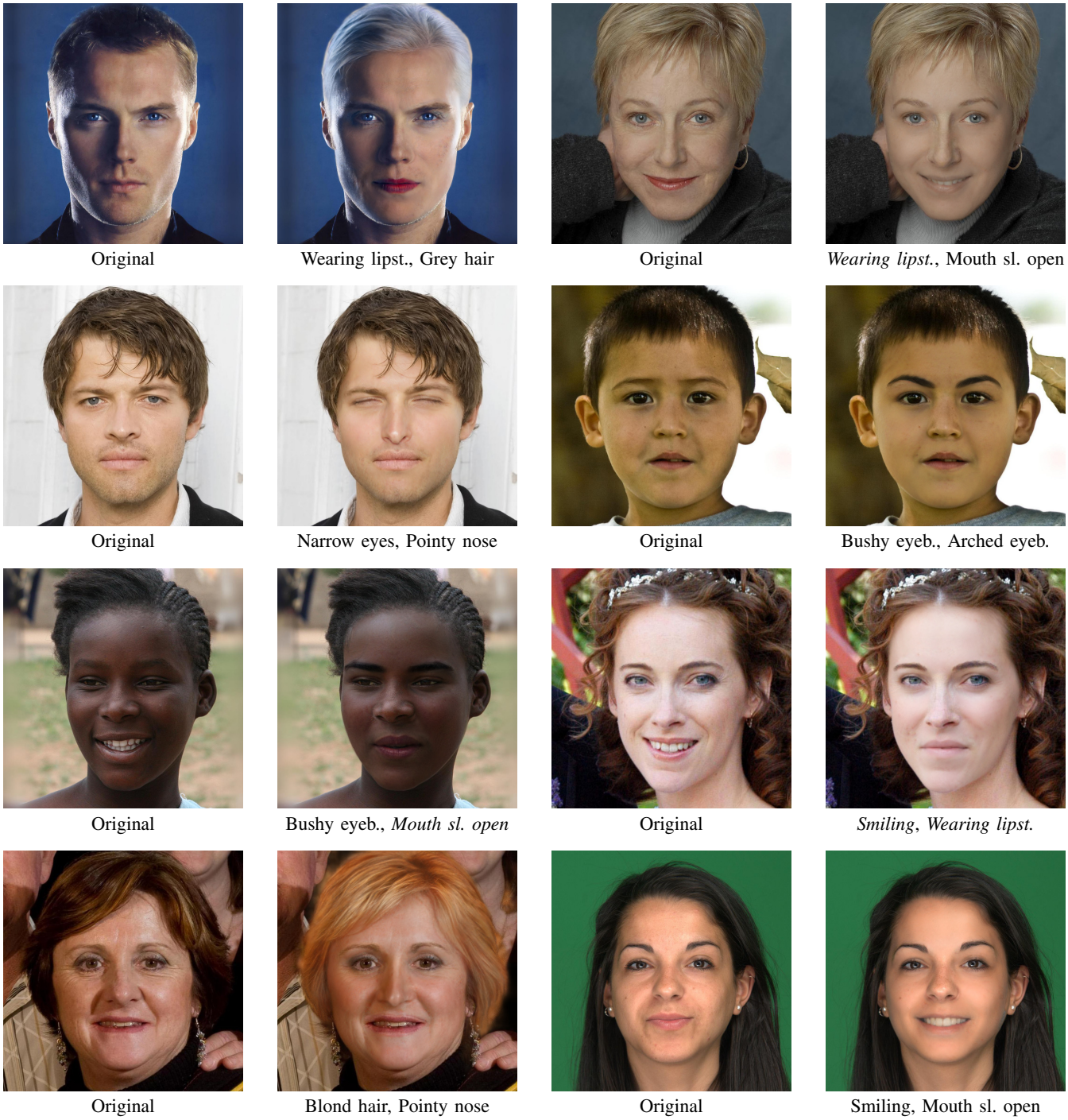

Fig. 21: Visual examples of image editing using MaskFaceGAN where multiple attributes are edited with a single optimization procedure. The presented examples show results when editing two attributes at the same time. Note that even for cases when the attributes correspond to the same spatial region, the generated results appear realistic and exhibit minimal distortions. Inverted (removed) attributes are displayed in italic.

datasets.

The FID scores calculated for the ablation study are presented in Table VIII. We observe that the noise optimization procedure improves the FID scores of every attribute. This can be attributed to the fact that noise optimization further optimizes the quality of the embedded image as well as generates high frequency image details, such as hair. The inclusion of the shape term λ_S only affects attributes associated with the hair region. Most of these attributes achieve a significantly lower FID score when the shape term is included in the loss function. This can be attributed to the more natural looking blending procedure, since the hair components from the generated and the original image are spatially aligned.

TABLE VIII: Ablation study results on CelebA–HQ. Reported are FID scores computed for each targeted attribute separately (↓ – lower is better). Note that both the noise optimization procedure as well as the shape term contribute toward higher quality results. The shape term affects only editing procedures associated with the hair region.

Target Attribute	FID scores ↓		
	$n = 0, \lambda_S = 0$	$\lambda_S = 0$	MaskFaceGAN
Arched eyebrows	49.69	24.17	24.17
Big nose	44.59	19.84	19.84
Black hair	78.77	55.27	43.39
Brown hair	72.14	50.53	37.12
Bushy eyebrows	52.67	22.80	22.80
Grey hair	81.35	47.98	37.47
Mouth sl. open	46.24	23.27	23.27
Narrow eyes	61.89	28.69	28.69
Pointy nose	47.47	23.38	23.38
Smiling	46.91	23.87	23.87
Straight hair	75.23	54.58	52.58
Wavy hair	73.00	52.00	59.83
Wearing lipstick	48.79	26.93	26.93

B. FID results

The FID score is used as a measure of quality for the edited images. FID scores, grouped by attributes, are shown in Tables IX, X and XI for CelebAHQ, Helen and Siblings dataset, respectively.

Note that MaskFaceGAN outperforms all competing models with a significant margin at all attributes except when editing "Straight hair" and "Wavy hair" attributes. For these attributes, STGAN achieves better results than MaskFaceGAN. The single–attribute editing results shown in Figs. 15, 16 and 17 show that STGAN only slightly changes the hair shape, which preserves the quality of the initial image – but at the cost of a convincing semantic presence of the targeted attribute. MaskFaceGAN, on the other hand, generates stronger semantic content, but also hallucinates some of the image details.

C. User Study Results

Similarly as in the main part of the paper, we report user study scores for two experiments in this section: (i) in the first, users were asked to rate editing results on a 5–point Likert scale, and (ii) in the second, users were asked to select the best result among the edited images generated by the evaluated models.

The results for model ratings are shown in Tables XII, XIII and XIV for the CelebAHQ, Helen and Siblings datasets, respectively and the results for the best model selection ratings are shown in Tables XV, XVI and XVII with the same dataset order. The proposed MaskFaceGAN model is consistently rated higher than other models on most of the considered attributes with the notable exception of "Narrow eyes" attribute, where AttGAN achieves better performance across all datasets. The difference most likely stems from the MaskFaceGAN tendency to close the eyes instead of narrowing them. A similar effect can also be observed in Figs. 15, 16 and 17 for the InterFaceGAN and InterFaceGAN–D results.

XI. User Study Details

The user study was performed on the Amazon Mechanical Turk platform. Access was only granted to "Master workers", that is, the workers that have had good performance on other tasks at that time. All images shown were of the same resolution (1024×1024) to discourage annotation based on resolution. Lower resolution images were resampled using bilinear interpolation. The question posed to worker was *"Choose the image that changes the attribute more successfully, is of higher image quality and better preseres the identity and fine details of the source image"*. The workers then had to score image edit of each of the model. The images were reshuffled for every worker task to avoid cheating.

XII. Implementation Details

XIII. Encoder-decoder methods (StarGAN, AttGAN, STGAN)

For encoder-decoder methods, we strictly follow the implementation details, as specified by the source code of each model. The only hyperparameter specified is the input and output resolution of each model. For StarGAN model, the highest suggested resolution (256×256) resulted in high frequency of visual degradation in the edited images. We therefore train a smaller resolution model (128×128) that performs better. For AttGAN and STGAN model, we chose the highest proposed resolution, that is 384×384.

XIV. InterFaceGAN

Our InterFaceGAN method is implemented in the latent space of our GAN model. We follow the procedure as outlined by the paper [9]; first, we generate 500,000 pairs of latent code w and corresponding image. The classifier scores the facial attribute of each image and top 10,000 positive and negative samples are kept. Linear SVM is applied on the latent codes of these images to obtain the normal vector of the hyperplane. The SVM regularization term is set to 1.

One must specify the magnitude of movement in the latent space for the InterFace method. A small magnitude barely changes the presence/absence of a facial attribute, but preserves the face identity. A large magnitude tends to make large changes that correspond to the desired facial attribute edit, however it usually comes at the cost of an identity change. We visualized results for several different magnitudes and chose 1 as the optimal value.

XV. INTERFACEGAN–D

When implementing the disentangled version of InterFaceGAN model, denoted as InterFaceGAN–D, one can choose multiple attributes that can be disentangled from some target attribute edit. In our experiments, we found that disentanglement works best when disentangling only a single attribute, i.e. with a simple vector projection method as described in [9]. When choosing the attribute to disentangle for a given target attribute, we choose the attribute that displays the most entanglement issues in the generated results. For the attributes, where entanglement was not that problematic or the target attribute is hard to specify, the most correlated attribute (positive or negative correlation) from the CelebA–HQ training dataset was chosen. The disentangled attributes are presented in Table XVIII.

TABLE IX: FID scores per attribute computed for the CelebA-HQ dataset – lower is better. The table shows a comparison with competing state–of–the–art models. The best score for each attribute is highlighted in bold.

Attribute	StarGAN	AttGAN	STGAN	InterFaceGAN	InterFaceGAN–D	MaskFaceGAN
Arched eyebrows	133.49	52.22	40.34	73.01	77.77	**24.17**
Big nose	137.24	57.78	46.94	82.30	76.20	**19.84**
Black hair	143.31	77.26	57.05	80.51	77.57	**43.39**
Brown hair	140.61	58.88	46.88	72.97	75.21	**37.12**
Bushy eyebrows	125.90	50.67	38.22	78.34	74.31	**22.80**
Grey hair	172.74	139.82	98.05	98.45	78.50	**37.47**
Mouth slightly open	137.74	61.47	38.75	80.88	76.24	**23.27**
Narrow eyes	137.76	61.63	39.42	82.20	77.63	**28.69**
Pointy nose	131.32	50.51	39.15	73.41	73.87	**23.38**
Smiling	141.69	61.63	42.83	78.88	75.41	**23.87**
Straight hair	137.27	60.57	**43.62**	73.65	76.94	52.58
Wavy hair	143.40	67.06	**48.65**	73.62	75.24	59.83
Wearing lipstick	148.91	78.70	63.99	89.00	84.45	**26.93**

TABLE X: FID scores per attribute computed for the Helen dataset – lower is better. The table shows a comparison with competing state–of–the–art models. The best score for each attribute is highlighted in bold.

Attribute	StarGAN	AttGAN	STGAN	InterFaceGAN	InterFaceGAN–D	MaskFaceGAN
Arched eyebrows	148.26	68.22	47.38	87.90	91.24	**21.65**
Big nose	145.10	70.57	56.79	94.05	90.71	**19.19**
Black hair	151.61	85.47	60.52	92.19	92.26	**42.74**
Brown hair	149.86	70.38	52.14	87.42	89.12	**37.88**
Bushy eyebrows	145.54	66.99	44.20	89.00	91.61	**21.29**
Grey hair	180.83	140.68	102.65	102.65	91.60	**43.04**
Mouth slightly open	150.45	72.40	46.06	88.16	89.00	**21.87**
Narrow eyes	154.31	81.84	50.00	90.56	93.07	**23.67**
Pointy nose	147.12	66.93	49.04	84.23	89.09	**20.98**
Smiling	150.66	74.05	48.94	90.17	88.20	**22.47**
Straight hair	148.26	78.32	**55.92**	88.24	92.06	66.85
Wavy hair	161.97	81.34	**65.33**	89.95	90.39	76.04
Wearing lipstick	150.33	81.43	67.74	97.29	93.76	**24.33**

TABLE XI: FID scores per attribute computed for the SiblingsDB-HQf dataset – lower is better. The table shows a comparison with competing state–of–the–art models. The best score for each attribute is highlighted in bold.

Attribute	StarGAN	AttGAN	STGAN	InterFaceGAN	InterFaceGAN–D	MaskFaceGAN
Arched eyebrows	181.24	66.69	38.29	75.42	81.55	**29.95**
Big nose	166.84	68.64	43.69	85.97	80.07	**16.93**
Black hair	176.82	87.83	49.60	85.91	83.24	**37.45**
Brown hair	175.56	64.17	37.08	78.72	81.90	**31.92**
Bushy eyebrows	171.77	62.65	32.34	81.63	82.24	**28.43**
Grey hair	199.54	141.63	106.99	90.54	83.61	**36.37**
Mouth slightly open	173.15	76.05	36.66	82.04	86.61	**23.80**
Narrow eyes	182.95	94.33	39.37	84.46	87.40	**35.49**
Pointy nose	169.58	67.07	36.67	77.21	81.77	**24.55**
Smiling	175.40	82.80	43.63	75.63	81.38	**22.81**
Straight hair	172.94	76.65	**49.29**	74.36	81.75	59.24
Wavy hair	184.82	84.39	**62.69**	77.47	84.81	70.06
Wearing lipstick	168.28	84.55	59.19	91.06	87.84	**31.84**

TABLE XII: Results of the user study on test images from the CelebA–HQ dataset. Users were asked to rate the models on a 5–point Likert scale, where 5 stands for a perfect result. The model with the best user rating for each attribute is presented in bold.

Attribute	StarGAN	AttGAN	STGAN	InterFaceGAN	InterFaceGAN–D	MaskFaceGAN
Arched eyebrows	1.44 ± 0.94	2.75 ± 0.96	3.00 ± 1.02	3.05 ± 1.03	3.38 ± 1.19	$\mathbf{4.03 \pm 1.24}$
Big nose	1.37 ± 0.84	3.09 ± 1.05	2.87 ± 0.96	2.72 ± 0.99	2.60 ± 0.99	$\mathbf{4.35 \pm 1.14}$
Black hair	1.68 ± 1.02	2.74 ± 1.23	3.02 ± 1.12	3.16 ± 0.81	3.50 ± 1.06	$\mathbf{4.00 \pm 1.23}$
Blond hair	1.74 ± 1.15	2.81 ± 1.15	2.97 ± 1.06	2.98 ± 1.02	3.24 ± 1.06	$\mathbf{4.12 \pm 1.12}$
Brown hair	1.39 ± 0.82	2.73 ± 1.10	3.00 ± 0.98	3.13 ± 0.95	3.37 ± 0.97	$\mathbf{4.41 \pm 0.86}$
Bushy eyebrows	1.63 ± 1.21	2.61 ± 1.12	3.18 ± 0.97	3.17 ± 0.95	3.53 ± 1.03	$\mathbf{4.42 \pm 1.17}$
Grey hair	1.41 ± 0.84	3.15 ± 1.15	2.58 ± 1.11	2.10 ± 1.15	2.07 ± 1.18	$\mathbf{3.91 \pm 1.22}$
Mouth slightly open	1.27 ± 0.57	2.97 ± 1.21	2.88 ± 0.93	2.44 ± 1.10	2.68 ± 1.30	$\mathbf{4.11 \pm 1.28}$
Narrow eyes	1.38 ± 0.86	$\mathbf{3.60 \pm 1.27}$	3.00 ± 1.08	2.52 ± 0.98	2.62 ± 1.11	3.52 ± 1.46
Pointy nose	1.63 ± 1.09	3.00 ± 1.09	3.00 ± 0.96	3.14 ± 1.05	3.41 ± 1.15	$\mathbf{4.34 \pm 1.01}$
Smiling	1.36 ± 0.89	2.84 ± 1.20	3.17 ± 1.08	2.66 ± 1.12	2.80 ± 1.31	$\mathbf{4.11 \pm 1.18}$
Straight hair	1.31 ± 0.81	3.05 ± 1.04	3.36 ± 1.02	3.12 ± 0.94	3.64 ± 1.03	$\mathbf{3.80 \pm 1.28}$
Wavy hair	1.52 ± 0.97	2.71 ± 0.93	3.13 ± 1.01	3.05 ± 1.18	3.31 ± 1.27	$\mathbf{3.74 \pm 1.32}$
Wearing lipstick	1.27 ± 0.72	3.17 ± 1.13	2.89 ± 1.16	2.67 ± 0.85	2.80 ± 1.08	$\mathbf{4.04 \pm 1.35}$

TABLE XIII: Results of the user study on test images from the Helen dataset. Users were asked to rate the models on a 5–point Likert scale, where 5 stands for a perfect result. The model with the best user rating for each attribute is presented in bold.

Attribute	StarGAN	AttGAN	STGAN	InterFaceGAN	InterFaceGAN–D	MaskFaceGAN
Arched eyebrows	1.46 ± 0.88	2.79 ± 1.18	2.95 ± 1.06	2.53 ± 0.94	2.72 ± 1.09	$\mathbf{4.10 \pm 1.15}$
Big nose	1.25 ± 0.58	2.92 ± 1.15	3.07 ± 1.07	2.16 ± 0.88	2.42 ± 1.00	$\mathbf{4.39 \pm 0.89}$
Black hair	1.44 ± 0.76	2.54 ± 1.19	3.24 ± 1.19	2.79 ± 0.91	2.89 ± 1.12	$\mathbf{3.64 \pm 1.28}$
Blond hair	1.30 ± 0.55	2.73 ± 1.18	2.92 ± 1.14	2.88 ± 1.11	2.71 ± 1.05	$\mathbf{3.66 \pm 1.14}$
Brown hair	1.36 ± 0.65	2.70 ± 1.22	2.59 ± 1.08	3.00 ± 1.07	2.79 ± 1.11	$\mathbf{4.05 \pm 1.18}$
Bushy eyebrows	1.37 ± 0.72	2.35 ± 1.23	3.13 ± 1.21	2.40 ± 1.02	2.67 ± 1.14	$\mathbf{3.93 \pm 1.21}$
Grey hair	1.34 ± 0.65	2.74 ± 1.21	2.77 ± 1.20	1.94 ± 1.02	2.07 ± 1.06	$\mathbf{3.65 \pm 1.34}$
Mouth slightly open	1.24 ± 0.58	2.78 ± 1.32	3.14 ± 1.22	1.98 ± 0.88	2.12 ± 1.07	$\mathbf{3.73 \pm 1.51}$
Narrow eyes	1.32 ± 0.61	$\mathbf{3.18 \pm 1.43}$	2.98 ± 1.34	1.84 ± 0.92	1.65 ± 0.77	2.99 ± 1.38
Pointy nose	1.16 ± 0.52	3.02 ± 1.11	3.16 ± 1.04	2.56 ± 0.98	2.70 ± 0.95	$\mathbf{4.30 \pm 0.96}$
Smiling	1.15 ± 0.41	2.82 ± 1.49	$\mathbf{3.55 \pm 1.33}$	2.15 ± 1.03	2.14 ± 1.11	3.43 ± 1.33
Straight hair	1.42 ± 0.71	3.14 ± 1.01	$\mathbf{3.36 \pm 1.22}$	2.39 ± 1.01	2.62 ± 1.19	3.23 ± 1.32
Wavy hair	1.27 ± 0.63	2.64 ± 1.06	2.92 ± 1.13	2.52 ± 1.17	2.28 ± 1.16	$\mathbf{4.05 \pm 1.14}$
Wearing lipstick	1.19 ± 0.48	2.62 ± 1.21	2.65 ± 1.21	2.34 ± 0.98	2.37 ± 1.08	$\mathbf{4.08 \pm 1.20}$

TABLE XIV: Results of the user study on test images from the SiblingsDB–HQf dataset. Users were asked to rate the models on a 5–point Likert scale, where 5 stands for a perfect result. The model with the best user rating for each attribute is presented in bold.

Attribute	StarGAN	AttGAN	STGAN	InterFaceGAN	InterFaceGAN–D	MaskFaceGAN
Arched eyebrows	1.48 ± 0.78	3.00 ± 1.15	3.27 ± 1.01	2.43 ± 0.90	2.64 ± 0.96	$\mathbf{4.14 \pm 1.12}$
Big nose	1.51 ± 0.87	3.15 ± 1.13	3.00 ± 0.86	2.29 ± 0.81	2.50 ± 0.88	$\mathbf{4.27 \pm 1.03}$
Black hair	1.55 ± 0.88	2.99 ± 1.10	$\mathbf{3.64 \pm 1.08}$	2.75 ± 0.87	3.15 ± 1.03	3.60 ± 1.12
Blond hair	1.62 ± 0.88	3.10 ± 1.15	3.20 ± 0.97	2.71 ± 0.86	2.97 ± 0.87	$\mathbf{3.82 \pm 1.15}$
Brown hair	1.67 ± 1.02	3.13 ± 1.12	3.14 ± 0.94	2.94 ± 0.94	3.04 ± 1.04	$\mathbf{3.62 \pm 1.10}$
Bushy eyebrows	1.42 ± 0.73	2.93 ± 1.08	3.27 ± 1.02	2.57 ± 0.98	2.97 ± 1.06	$\mathbf{3.92 \pm 1.23}$
Grey hair	1.72 ± 1.10	3.05 ± 1.11	2.99 ± 0.98	2.30 ± 0.96	2.40 ± 1.03	$\mathbf{3.55 \pm 1.30}$
Mouth slightly open	1.47 ± 0.88	3.11 ± 1.15	3.38 ± 0.95	2.08 ± 0.86	2.14 ± 0.93	$\mathbf{4.15 \pm 1.18}$
Narrow eyes	1.50 ± 0.89	$\mathbf{3.39 \pm 1.23}$	3.23 ± 1.19	2.20 ± 0.97	2.20 ± 0.95	3.20 ± 1.29
Pointy nose	1.43 ± 0.79	3.20 ± 1.11	3.32 ± 0.98	2.61 ± 0.84	2.91 ± 1.04	$\mathbf{4.20 \pm 1.03}$
Smiling	1.38 ± 0.85	3.04 ± 1.04	3.84 ± 0.97	2.36 ± 0.81	2.46 ± 0.84	$\mathbf{4.11 \pm 0.99}$
Straight hair	1.51 ± 0.85	3.27 ± 0.98	3.34 ± 1.07	2.67 ± 0.90	2.77 ± 0.96	$\mathbf{3.47 \pm 1.22}$
Wavy hair	1.53 ± 0.93	3.19 ± 1.10	3.35 ± 1.13	2.50 ± 0.93	2.56 ± 1.08	$\mathbf{3.70 \pm 1.21}$
Wearing lipstick	1.53 ± 1.00	3.15 ± 0.96	3.17 ± 1.02	2.33 ± 0.89	2.54 ± 1.07	$\mathbf{4.16 \pm 1.12}$

TABLE XV: Results of the user study on test images from the CelebA–HQ dataset in terms of percentage of selected images. Users were asked to select the best editing results when presented with image examples generated by all evaluated models. The model with the best user rating for each attribute is presented in bold.

Attribute	StarGAN	AttGAN	STGAN	InterFaceGAN	InterFaceGAN–D	MaskFaceGAN
Arched eyebrows	1.43%	4.29%	7.14%	7.14%	24.29%	**55.71%**
Big nose	8.82%	10.29%	1.47%	2.94%	1.47%	**75.00%**
Black hair	6.15%	3.08%	7.69%	3.08%	26.15%	**53.85%**
Blond hair	5.71%	4.29%	8.57%	7.14%	18.57%	**55.71%**
Brown hair	2.94%	1.47%	2.94%	4.41%	16.18%	**72.06%**
Bushy eyebrows	3.12%	3.12%	4.69%	1.56%	9.38%	**78.12%**
Grey hair	3.08%	12.31%	10.77%	6.15%	10.77%	**56.92%**
Mouth slightly open	0.00%	11.43%	4.29%	2.86%	12.86%	**68.57%**
Narrow eyes	0.00%	**42.65%**	10.29%	1.47%	7.35%	38.24%
Pointy nose	1.45%	11.59%	2.90%	1.45%	13.04%	**69.57%**
Smiling	5.80%	8.70%	13.04%	2.90%	5.80%	**63.77%**
Straight hair	1.47%	8.82%	11.76%	14.71%	20.59%	**42.65%**
Wavy hair	1.52%	6.06%	6.06%	9.09%	19.70%	**57.58%**
Wearing lipstick	0.00%	11.76%	13.24%	4.41%	8.82%	**61.76%**

TABLE XVI: Results of the user study on test images from the Helen dataset in terms of percentage of selected images. Users were asked to select the best editing results when presented with image examples generated by all evaluated models. The model with the best user rating for each attribute is presented in bold.

Attribute	StarGAN	AttGAN	STGAN	InterFaceGAN	InterFaceGAN–D	MaskFaceGAN
Arched eyebrows	3.74%	14.95%	9.35%	5.61%	9.35%	**57.01%**
Big nose	7.62%	13.33%	11.43%	5.71%	5.71%	**56.19%**
Black hair	3.74%	11.21%	19.63%	9.35%	15.89%	**40.19%**
Blond hair	0.93%	10.28%	16.82%	16.82%	14.02%	**41.12%**
Brown hair	7.55%	9.43%	7.55%	8.49%	6.60%	**60.38%**
Bushy eyebrows	0.00%	11.43%	20.00%	6.67%	9.52%	**52.38%**
Grey hair	9.43%	6.60%	19.81%	5.66%	6.60%	**51.89%**
Mouth slightly open	0.96%	17.31%	22.12%	2.88%	6.73%	**50.00%**
Narrow eyes	0.00%	**47.17%**	22.64%	4.72%	1.89%	23.58%
Pointy nose	1.89%	7.55%	9.43%	7.55%	8.49%	**65.09%**
Smiling	0.00%	25.47%	**45.28%**	0.94%	6.60%	21.70%
Straight hair	0.93%	16.82%	**32.71%**	7.48%	12.15%	29.91%
Wavy hair	0.00%	3.85%	11.54%	6.73%	9.62%	**68.27%**
Wearing lipstick	1.90%	10.48%	12.38%	2.86%	8.57%	**63.81%**

TABLE XVII: Results of the user study on test images from the SiblingsDB–HQf dataset in terms of percentage of selected images. Users were asked to select the best editing results when presented with image examples generated by all evaluated models. The model with the best user rating for each attribute is presented in bold.

Attribute	StarGAN	AttGAN	STGAN	InterFaceGAN	InterFaceGAN–D	MaskFaceGAN
Arched eyebrows	2.11%	10.56%	14.79%	4.23%	8.45%	**59.86%**
Big nose	7.04%	4.23%	6.34%	6.34%	5.63%	**70.42%**
Black hair	2.80%	10.49%	**32.17%**	4.90%	31.47%	18.18%
Blond hair	4.26%	5.67%	12.77%	11.35%	15.60%	**50.35%**
Brown hair	11.43%	14.29%	5.71%	8.57%	17.14%	**42.86%**
Bushy eyebrows	2.13%	10.64%	15.60%	7.09%	16.31%	**48.23%**
Grey hair	5.59%	11.89%	8.39%	10.49%	13.99%	**49.65%**
Mouth slightly open	1.41%	7.04%	15.49%	4.93%	4.93%	**66.20%**
Narrow eyes	4.32%	30.22%	**33.81%**	5.76%	1.44%	24.46%
Pointy nose	3.57%	10.71%	6.43%	5.71%	23.57%	**50.00%**
Smiling	2.84%	3.55%	**63.12%**	1.42%	0.71%	28.37%
Straight hair	2.86%	20.00%	25.00%	7.14%	9.29%	**35.71%**
Wavy hair	3.55%	5.67%	13.48%	3.55%	13.48%	**60.28%**
Wearing lipstick	5.76%	6.47%	10.07%	7.91%	14.39%	**55.40%**

TABLE XVIII: Implementation details for the InterFaceGAN–D model used in experiments. The table shows which attribute was disentangled for a given target attribute. The target attributes presented in italic font denote the attributes, for which the disentangled attribute was selected based on the maximum absolute correlation of the CelebA training dataset.

Target attribute	**Disentangled attribute**
Arched eyebrows	Male
Big nose	Chubby
Black hair	Pale skin
Blond hair	Pale skin
Brown hair	Pale skin
Bushy eyebrows	Mustache
Grey hair	Young
Mouth slightly open	Smiling
Narrow eyes	Bald
Pointy nose	Rosy cheeks
Smiling	Mouth slightly open
Straight hair	Bald
Wavy hair	Heavy makeup
Wearing lipstick	Male